university of groningen

faculty of mathematics and natural sciences

Monodromy in Hamiltonian systems

Bachelor Project Physics & Mathematics

July 2015

Student: E.J. Pap

Supervisor Mathematics: Prof.dr. H. Waalkens

Supervisor Physics: Prof.dr. D. Boer

Abstract

Monodromy in Hamiltonian systems is the obstruction to the existence of globally defined smooth and single-valued action-angle variables. This subject in Hamiltonian mechanics has increased in attention in the past years. This thesis deals with an example system that exhibits monodromy; an idealized circularly symmetric microdisk with additional potential barrier inside. This system has billiard motion, and is proven to have monodromy in the fact that smooth and globally defined action variables need to be multi-valued. We find quantum monodromy in the quantum version confirmed by both the direct and WKB approximated spectra. Also an optical microresonator is investigated, but we see it has no monodromy unless a particular material can be made and used for it.

Keywords: Hamiltonian monodromy, quantum monodromy, billiard motion, action-angle variables

Contents

1 Introduction **4**

2 Monodromy **4**
2.1 Action-angle variables 5
2.2 Monodromy in Hamiltonian systems 9
2.3 Quantum monodromy 11
2.4 The monodromy matrix 15
2.5 Examples of monodromy in physical systems 16
2.6 Measuring monodromy 20

3 The radial square-well with barrier **24**
3.1 The quantum system 24
3.2 Phase portrait of classical analogue 26
3.3 Billiard motion 29
3.4 The spectrum 38

4 Optical Microresonator **48**
4.1 Introduction to optical microresonators 48
4.2 Solving the equations 51
4.3 Presence of monodromy 52

5 Conclusion **54**

6 References **55**

A Derivation of the billiard map **57**

1 Introduction

Monodromy is the obstruction to the existence of globally defined smooth and single-valued action-angle variables, or in quantum mechanics, an obstruction to likewise defined quantum numbers. This subject in Hamiltonian mechanics has drawn a lot of attention over the past years. Many systems are proven to have monodromy, and in this thesis, we look for it in special circularly symmetric planar systems.

This thesis consists of three parts together with the conclusion. Section 2 is an introduction to monodromy, while the other two sections implement this knowledge in two different systems.

We start the introduction to monodromy in Section 2.1 with action-angle variables, being a fundamental notion in this field. In Section 2.2 we will discuss its mathematical properties, while these classical notions are extended to quantum systems in Section 2.3. This is followed by a special consideration of the so-called monodromy matrix in Section 2.4, which appears in both classical and quantum mechanical systems. We end with some known examples of monodromy (Section 2.5) and discuss how to measure monodromy (Section 2.6). The mathematics is hence treated in Sections 2.1, 2.2 and 2.4, while Sections 2.3, 2.5 and 2.6 are specifically physics oriented. However, readers intending to skip one part are advised to still see the main points of the first four subsections of Section 2.

The concepts introduced will then enable us to delve deeper into a particular example in the next section. We take a modified microdisk as explained in Section 3.1, and first consider classical motions inside it. This is done using phase portraits in Section 3.2 and rigorous treatment of the action-angle variables in Section 3.3. Finally we compute the spectrum of the system in Section 3.4. We will see that both classical and quantum mechanical monodromy are present.

Then, we move on to another system, which is an optical microresonator setting. We will first introduce these systems in Section 4.1, and discuss solutions of the Maxwell equations for a specific set-up in Section 4.2. We then move on to the classical analogue of the system instead of computing the spectrum, as this analogue will tell us that monodromy will not be present. This is contained in Section 4.3, where we discuss other possibilities by suggesting a modified set-up.

2 Monodromy

In this section, we will discuss what monodromy is, with a large role for action-angle coordinates. A very important result concerning Hamiltionian monodromy is the Liouville–Arnold theorem, which provides conditions that guarantee the existence of such

smooth coordinates. After discussing this theorem, the phenomenon of monodromy in Hamiltonian systems will be stated, where these systems are assumed to be time-independent. We start with classical systems, but will discuss ways to extend monodromy to quantum systems. This is followed by a special subsection dedicated to the monodromy matrix, after which we discuss examples and measurements connected to monodromy.

2.1 Action-angle variables

Monodromy can be well introduced once the reader knows action-angle variables. This concept forms a basis for further understanding, and this subsection introduces them. The connection to monodromy is by the so-called Liouville-Arnold theorem, which we will state after discussing its requirements.

Consider a one-dimensional Hamiltonian system that is independent of time. Our generalized coordinates are then (q, p) with their evolution given by the level curves of the Hamiltonian. In phase space, this can produce pictures as in Figure 2.1.

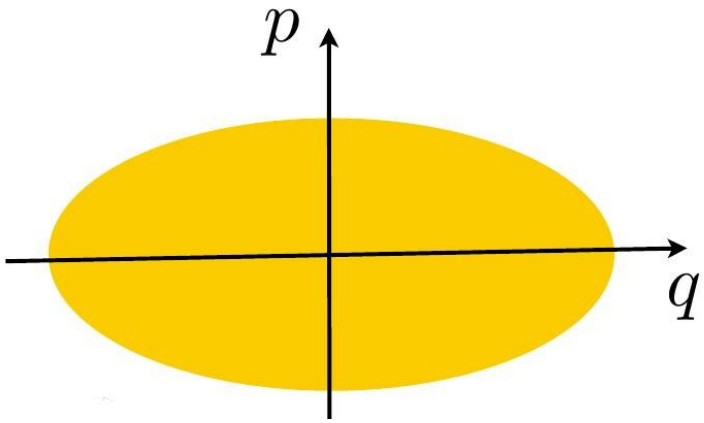

Figure 2.1: Example of phase space for a 1D Hamiltonian system [1]. The motion reduces to traversing the boundary of the ellipse. We note that a diagram showing the possible evolutions of (q, p) is called a phase portrait, which would consist of families of lines.

For the transformation, we can naturally get an angle by a parametrization of the ellipse. This path depends on a chosen value of the *constant of motion*; we denote the constant of motion (or *first integral*) by F, its value by f and the path by $\gamma(f)$. The action we define using the enclosed area, and becomes a line integral:

$$I(f) = \frac{1}{2\pi} \oint_{\gamma(f)} p dq.$$

To show the procedure, we discuss an example of the harmonic oscillator.

Example 2.1 (Harmonic Oscillator)**.**
The harmonic oscillator has Hamiltonian $H(q,p) = p^2/2m + kq^2/2$ and the solutions are, defining $\omega = \sqrt{k/m}$,

$$\begin{aligned} q &= A\sin(\omega t + \phi_0) \\ p &= m\omega A\cos(\omega t + \phi_0) \end{aligned} \tag{2.1}$$

where A is the amplitude and ϕ_0 the phase offset. The phase $\phi = \omega t + \phi_0$ defines naturally an angle variable, which tracks the position on the corresponding ellipse $H(q,p) = p^2/2m + kq^2/2 = h$ (which is our γ and we note it is diffeomorphic to a circle) in phase space. The action is then found using the integral, where the ellipse is parametrized by the solutions of the system (2.1).

$$\begin{aligned} I &= \frac{1}{2\pi}\oint_\gamma pdq = \frac{1}{2\pi}\int_0^{2\pi/\omega} m\omega A\cos(\omega t+\phi_0)d(A\sin(\omega t+\phi_0)) \\ &= \frac{m\omega^2A^2}{2\pi}\int_0^{2\pi/\omega}\cos^2(\omega t+\phi_0)dt = \frac{m\omega^2A^2}{2\pi}\frac{\pi}{\omega} = \frac{1}{2}m\omega A^2. \end{aligned}$$

So we see that $(q,p) \to \left(\phi, \frac{1}{2}m\omega A^2\right)$. The angle is the phase of the oscillator, and the action depends on the amplitude. The Hamiltonian can be rewritten in the new variables using that the energy at a turning point equals $H = \frac{1}{2}kA^2$ (so $A^2 = \frac{2I}{m\omega}$) and we see

$$H(I) = I\omega.$$

The motion becomes simple;

$$\begin{aligned} \frac{dI}{dt} &= \frac{\partial H}{\partial \phi} = 0 \\ \frac{d\phi}{dt} &= \frac{\partial H}{\partial I} = \omega. \end{aligned}$$

However, and this is a powerful property, we did not need to know the trajectory in analytic detail(!). Since $p = \sqrt{2m(E - kq^2/2)}$ and E is fixed, we get (setting $q_{\max} = \sqrt{2E/k}$):

$$I = \frac{1}{2\pi}\oint_\gamma \sqrt{2m(E-kq^2/2)}dq = \frac{\sqrt{2m}}{\pi}\int_{-q_{\max}}^{q_{\max}}\sqrt{E-kq^2/2}dq = E\sqrt{\frac{m}{k}} = E/\omega.$$

And we see that we get the same equation, using only the shape of the level curve as seen in the phase portrait (to identify the path γ). A similar procedure will be done when we consider frequencies of billiard motion in Section 3.3.

Having discussed this example, we would like a way to generalize this smooth behavior to higher dimensions. We will see that this is not always possible, where the Liouville-Arnold theorem will provide us with conditions, including the next definition.

Definition 2.1 (Involution)**.**
Given a Hamiltonian system and functions F_1 and F_2 on its phase space. The functions F_1 and F_2 are *in involution* if their Poisson bracket is zero:

$$\{F_1, F_2\} = 0.$$

In this language, F is a first integral of the system if and only if F is in involution with the Hamiltonian H (i.e. $\{F, H\} = 0$, or in other words, $\dot{F} = 0$ if $\dot{H} = 0$, where we assume $\dot{H} = 0$ for the system). In quantum physics, $\{F_1, F_2\} = 0$ is referred to as F_1 and F_2 *commute*, and the brackets correspond to the commutator $[F_1, F_2]$.

Another requirement of the theorem is the independence of the first integrals $F_1, \ldots, F_n$ on the phase space. In fact, for the case of monodromy, regions where this requirement does not hold are of interest, as will be explained after stating the theorem. At the moment we need to clarify what independence of the first integrals means.

Definition 2.2 (Independence of first integrals)**.**
The first integrals $F_1, \ldots, F_n$ of a Hamiltonian system are *independent* on a specified set U if the 1-forms $dF_1, \ldots, dF_n$ are linearly independent almost everywhere on U.

The theorem now states:

Theorem 1 (Liouville–Arnold [2])**.**
Given a Hamiltonian system with n degrees of freedom with phase space[1] Σ. Suppose that the system is integrable[2], that is:

- there exist n known first integrals $F_1, \ldots, F_n$ that are in involution.
- these first integrals are independent on the phase space Σ.

Let the vector $\boldsymbol{f}$ contain chosen (fixed) values of the first integrals, and consider then a common level set defined by

$$M_{\boldsymbol{f}} = \{(\boldsymbol{q}, \boldsymbol{p}) \in \Sigma : F_i(\boldsymbol{q}, \boldsymbol{p}) = (\boldsymbol{f})_i, i = 1, \ldots, n\}.$$

Suppose that $dF_1, \ldots, dF_n$ are independent everywhere on this set. Then:

1. $M_{\boldsymbol{f}}$ is a smooth manifold
2. If the manifold $M_{\boldsymbol{f}}$ is compact, then it is diffeomorphic to the n-dimensional torus $(\mathbb{S}^1)^n$.

[1] This corresponding phase space Σ should be a *symplectic manifold*. This means the manifold is smooth and is equipped with a closed and nondegenerate 2-form (which is called a symplectic form). However, we will not use this detail in later stages. Note that with phase space we mean the space containing both $\boldsymbol{q}$ and $\boldsymbol{p}$)

[2] Note that this is a rather special situation as not that many systems have as many constants of motion as degrees of freedom.

3. Action-angle variables exists in a neighborhood and their phase flow is linear in time. That is, if the angles are $\phi_1, \ldots, \phi_n$, we have $\phi_i(t) = \omega_i t + \phi_i(0)$ for $i = 1, \ldots, n$ where the frequencies ω_i depend on $\boldsymbol{f}$.

4. The canonical equations with Hamiltonian H can be integrated by quadratures.

As in [3], one can rephrase some essential points of the theorem: if a connected component of the common level set is bounded and regular (so the gradients of the constants of motion are linearly independent), then the component has the topology of a torus and action-angle variables exist in a neighborhood of the torus.

The mentioned action-angle variables can then be obtained in a similar way as before for higher dimensions. The greatest change lies in the paths. In this thesis, paths are obvious (like the ellipse) or one can use coordinate lines. Otherwise, one can really decompose the torus, as is illustrated in Figure 2.2.

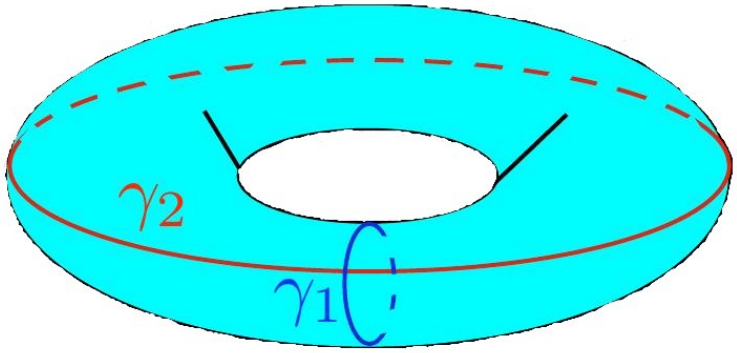

Figure 2.2: Decomposition of a 2-torus into two different paths [1].

Definition 2.3 (Action-angle variables)**.**
Given a Hamiltonian system with n degrees of freedom, and hence with a $2n$ dimensional phase space. *Action-angle variables* are then variables $(\boldsymbol{I}, \boldsymbol{\phi})$, obtained from a canonical transformation. These depend on the chosen motion in phase space, which we assume to be labeled by n values of first integrals $F_1, \ldots, F_n$. The values define the n-dimensional vector $\boldsymbol{f}$ where $(\boldsymbol{f})_i = F_i$.
Let $\phi_1, \ldots, \phi_n$ be the angle-variables corresponding to the n-dimensional torus diffeomorphic to the state space of the system[3]. Let $\gamma_1, \ldots, \gamma_n$ form a basis for the one-dimensional cycles on the torus, such that the increase of ϕ_i along γ_j equals $2\pi\delta_{ij}$.
The action variables are then obtained using:

$$I_i(\boldsymbol{f}) = \frac{1}{2\pi} \oint_{\gamma_i(\boldsymbol{f})} \boldsymbol{p} \cdot d\boldsymbol{q}.$$

[3]This is possible by the Liouville-Arnold theorem.

The Hamiltonian is then a function of the actions alone, and hence the system gets the following form:

$$\frac{d\boldsymbol{I}}{dt} = -\frac{\partial H}{\partial \boldsymbol{\phi}} = 0$$
$$\frac{d\boldsymbol{\phi}}{dt} = \frac{\partial H}{\partial \boldsymbol{I}} := \boldsymbol{\omega}(\boldsymbol{I}).$$

That is, all actions $I_1, \ldots, I_n$ are constant in time and the n angles change linearly in time ($\phi_i(t) = \phi_i(0) + \omega_i t$).

Yet we can make the connection to monodromy. We saw that Theorem 1 guarantees locally smooth action-angle variables. Imagine that we have a closed loop in constant of motion space, while each point has a such a neighborhood. Can we then introduce action-angle variables defined smoothly[4] across the whole loop? The answer is: not necessarily. As we will see, when the path encloses a 'singularity', we can't. If not, we can.

Theorem 1 applies in the neighborhoods of regular points of the energy-momentum mapping [4] (more in next subsection). It is not surprising then that monodromy may occur at the critical points of this mapping. An example of this is the spherical pendulum, which we will discuss on page 16. We will see that the standing-up position, where the gradients of energy and angular momentum become dependent, corresponds to the location 'generating' monodromy. More on this system can be found in [5, 6]. Another example is a particle approaching a circular symmetric potential bump, where on top the gradient vectors are linearly dependent [3].

2.2 Monodromy in Hamiltonian systems

Monodromy is used in multiple places, the word itself just meaning 'once around'. In the present context, we often go around a singularity, which will manifest itself after closing your path. In this thesis we concern ourselves with the monodromy in time-independent two degree-of-freedom Hamiltonian systems[5]. Having introduced the action-angle variables and the Liouville–Arnold theorem, the definition for monodromy that is used in this thesis is easily understood. Where the Liouville–Arnold theorem guarantees smooth coordinates, monodromy is the phenomenon where it is impossible to define these in a smooth and single-valued way to describe the entirety of the system under consideration.

Formally, we state the definition obtained from [7]:

[4] We will use the word smooth for convenience, meaning continuously differentiable instead of infinitely differentiable.

[5] One dimensional systems, like the harmonic oscillator, will not have monodromy as there is no closed loop 'around' a point in one dimensional space.

Definition 2.4 (Monodromy)**.**
Monodromy in a system is an obstruction to the existence of global, smooth, and single-valued action variables.

Why the names 'regular value' and 'singularity' make sense can be explained with the energy-momentum map. This energy-momentum map $\mathcal{EM}$ is obtained by putting together the energy map $E(q,p)$ and the angular momentum map $L(q,p)$ to get

$$\begin{aligned}\mathcal{EM} : \Sigma &\to \mathbb{R}^2 \\ (q,p) &\mapsto (L(q,p), E(q,p)).\end{aligned}$$

We note that the codomain $\mathbb{R}^2$ may be replaced by $\mathbb{C}^2$ if needed. The symmetry of the image may follow from the fact that the system is isotropic, which is true for many simple examples. According to the Liouville-Arnold theorem, the pre-images of a value in energy-momentum space is diffeomorphic to a torus $\mathbb{T}^2$ (i.e. the configurations (q_1, q_2, p_1, p_2) with the chosen E and L are together like a torus) if the value is a regular value[6] of the energy-momentum map. Indeed, L and E are usually in involution for a two degree-of-freedom system and so we need only to consider whether their differentials are independent, which is equivalent to the value being regular. Hence, the singular values of this mapping are likely to have a pre-image not diffeomorphic to $\mathbb{T}^2$, but to a deformed or pinched torus (so containing a singular point).

If we mark the singular values, one can get pictures as in Figure 2.3, where the gray region contains the available states. In (a), we see the simplest case called an isolated singularity, while in (b), we see a continuum of singular points. The first case is called integer monodromy, and the pre-image of the singularity is a pinched torus like in Figure 2.4a. Many more deformed tori are possible, like in part (b) of the same picture.

For 2-dimensional systems, a ratio of frequencies can be calculated using the actions and it will prove very useful later on. This ratio is called the winding number W, and the calculation follows a simple notion, namely, we differentiate $H(I_1, I_2)$ (Hamiltonian written in action-variables, where the angles are cyclic, i.e. the Hamiltonian does not depend on them) with respect to angular momentum l while keeping the energy constant. The answer is zero as $H = E = \text{constant}$, but we can write

$$\begin{aligned}\frac{\partial}{\partial l} H(I_1, I_2) &= 0 \\ \implies \frac{\partial H}{\partial I_1}\frac{\partial I_1}{\partial l} + \frac{\partial H}{\partial I_2}\frac{\partial I_2}{\partial l} &= 0 \\ \implies \omega_1 \frac{\partial I_1}{\partial l} + \omega_2 \frac{\partial I_2}{\partial l} &= 0.\end{aligned}$$

[6] A value is regular if all points in its pre-image are regular, and is singular if at least one point in the pre-image is singular.

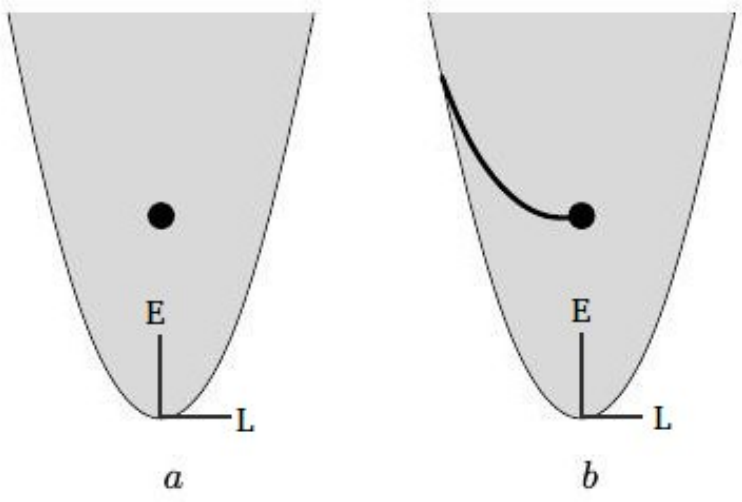

Figure 2.3: Typical images of the energy-momentum mapping [8], where the vertical axis represents energy and the horizontal axis the angular momentum. In (a), integer monodromy is shown. In (b), an example of a more complicated case of fractional monodromy is illustrated.

Hence, we conclude

$$W := \frac{\omega_2}{\omega_1} = -\left(\frac{\partial I_1}{\partial l}\right) / \left(\frac{\partial I_2}{\partial l}\right). \tag{2.2}$$

Research in monodromy started around 1980 with a paper by Duistermaat [9] and has become a lively field. Many classical systems, a famous example being the spherical pendulum [10], were found to have monodromy. This spread also into quantum theory, using the tools discussed in the next subsection.

2.3 Quantum monodromy

So far, we only considered classical systems where the states form a continuum and we could follow action-angle variables along smooth paths. In the quantum world, this is not possible, and so we must find an equivalent notion to extend monodromy to quantum systems.

As we deal only with two dimensional systems, the allowed states will form a grid/lattice in energy-momentum space using the energy-momentum map $\mathcal{EM}$. This grid can be superimposed on the 'parabolas' as in Figure 2.3. A similar grid is formed by finding two actions (note that L is already an action) and take the Cartesian product of these. We now consider a unit lattice cell/square in this lattice (following [11]). By the Bohr-

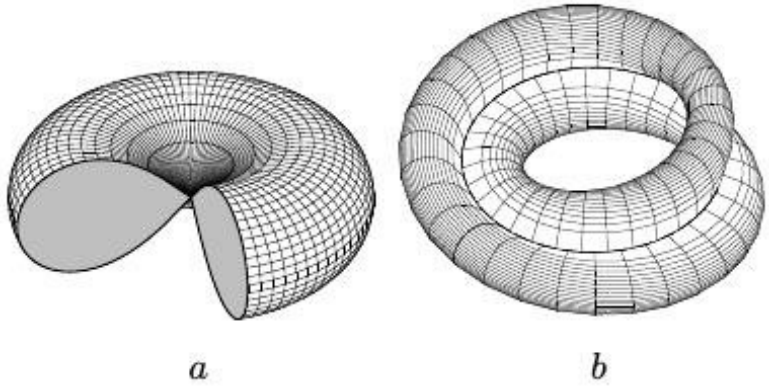

Figure 2.4: Tori representing the pre-images in (q_1, q_2, p_1, p_2)-space corresponding to monodromy in 2-dimensional Hamiltonian systems [8]. Note that the four dimensional phase space becomes two dimensional when also two constants of motion are fixed. The torus in (a) is pinched, while the torus in (b) is twisted. The torus in (a) is a possibility for the singularity for (a) in Figure 2.3, likewise for (b). However, other tori are also possible.

Sommerfield quantatization, the points are separated by widths[7] $\Delta I_1, \Delta I_2$ such that any point can be expressed as an initial point plus integer times these widths in the horizontal or vertical direction. These directions define a basis $\{e_1, e_2\}$, and so define a lattice cell marked by integer coordinates $\{(n_1, n_2), (n_1+1, n_2), (n_1, n_2+1), (n_1+1, n_2+1)\}$. Using the locally defined structure of the action-angle coordinates, this cell can be moved to a next by increasing appropriate integers by one.

If this structure exists globally, then any closed path will return the integers n_1, n_2 to their original values, meaning that the cell is unchanged. If however the cell is deformed, we know the structure cannot be globally defined, implying monodromy. Monodromy occurring in this manner is called *quantum monodromy*. However, this lattice can be mapped on the energy-momentum lattice, and so we can track a unit cell also in the energy-momentum spectrum. Notice that we then left the world of smooth classical functions and arrived at an interpretation suitable for a quantized state space. Hence, the moving cell is a way of showing quantum monodromy. To make this concept more precise, we state the following 'definition', inspired by [12].

Definition 2.5 (Quantum Monodromy)**.**
A quantum system has *quantum monodromy* if there is absence of a single, smoothly[8] varying set of quantum numbers.

[7] This is a semi-classical approximation of the exact quantum spectrum where the widths are integer or half-integer multiples of $\hbar$.

[8] In the context of changing the size of $\hbar$. Semi-classical pictures can for instance be obtained by letting $\hbar \to 0$.

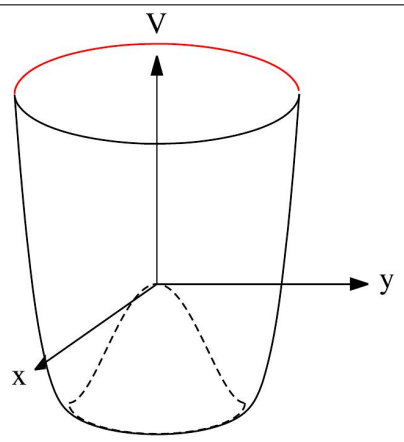

Figure 2.5: The potential, also known as the 'champagne bottle' or 'Mexican hat' potential [13]. Inside a disk it is equal to $-ar^2/2$ and infinite outside it.

To see both the moving cell argument together with smoothly defined quantum numbers in Definition 2.5, Figure 2.6 illustrates this nicely (where the potential is shown in Figure 2.5). On the left, there is no monodromy and most lines are smooth. On the right, monodromy is present and all lines show 'kinks' around $m = 0$. The only kink on the left arises from choosing $m \to -m$ symmetric quantum numbers, forcing a kink.

Note that the argument above does not depend on the cell chosen; we could also take a non-square cell to start with (as we will usually do in the energy-momentum case). However, we keep a cell with four vertexes, as two or three points may not be so clear to see deformation. We note that the different initial choices are related by matrices M with integer entries and determinant 1 to preserve independence, volume and orientation, i.e. $M \in SL(2, \mathbb{Z})$.

Numerous quantum systems have already been found exhibiting quantum monodromy ([8, 15, 16] and many more). We see that one can use the moving cell for the quantum system and the action-angle variables (together with the Liouville-Arnold theorem) in the classical system. Since there is a correspondence between classical en quantum systems, one can use both once a system is chosen. Such a procedure will be used in Section 3.

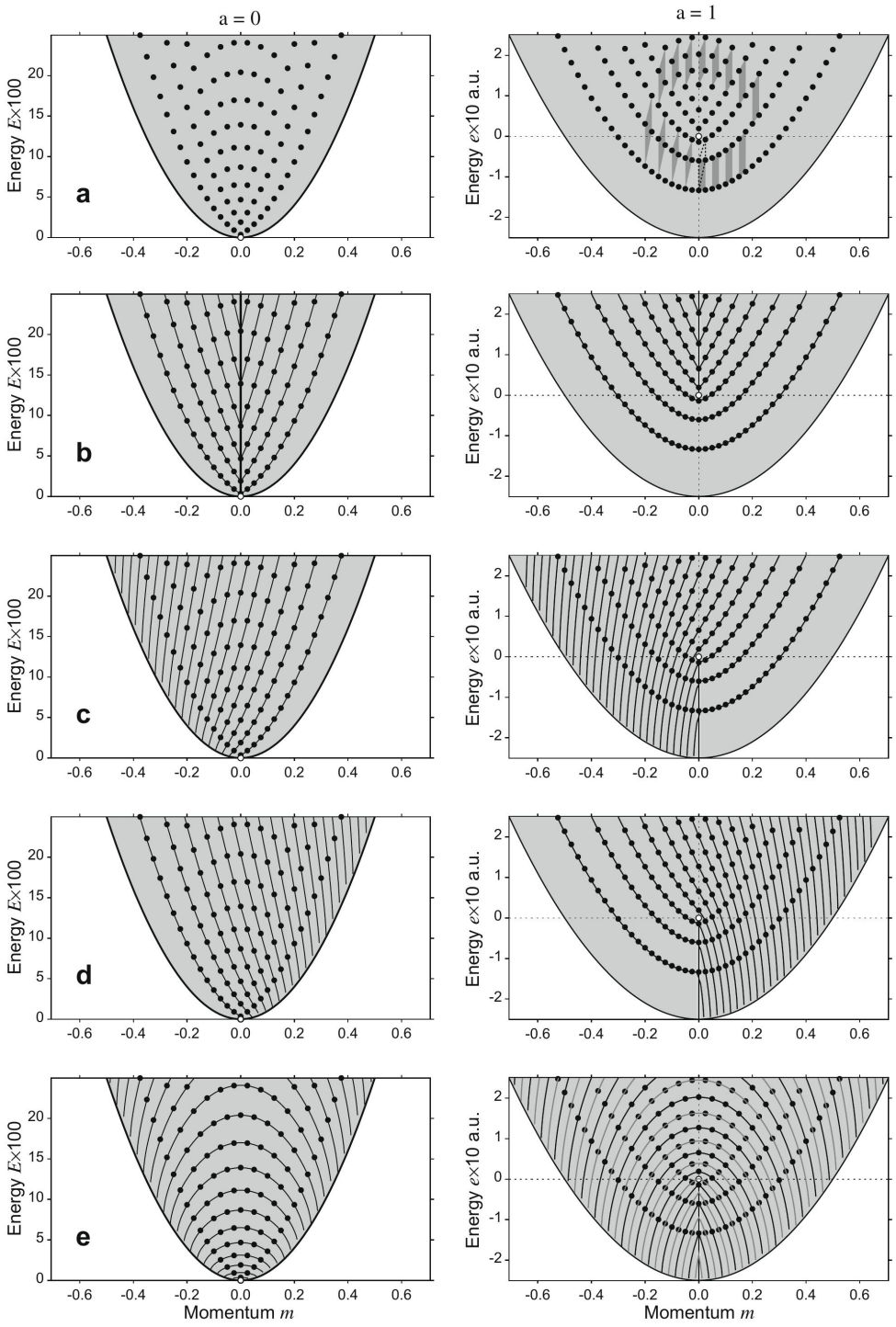

Figure 2.6: Smooth lines through quantum states on the left are deformed by introduction of monodromy on the right [14], with the potential defined in Figure 2.5. On the left, the potential is zero in the disk, and hence no barrier causing monodromy is present. It is present on the right.

2.4 The monodromy matrix

As mentioned, classical monodromy makes it impossible to connect action-angle variables smoothly, and we come back with different values. This must mean that the fundamental paths γ_i are mixed after one turn. As the paths determine the actions, also these transform according to a matrix. We will explain the meaning of this *monodromy matrix* in various settings below.

Concerning the paths for the action-integrals; if we start with paths[9] γ_1 and γ_2 and get new paths γ_1' and γ_2' after one turn, then these are related by the monodromy matrix M like:

$$\begin{pmatrix} \gamma_1' \\ \gamma_2' \end{pmatrix} = M \begin{pmatrix} \gamma_1 \\ \gamma_2 \end{pmatrix}.$$

The entries of M must be integers and the determinant is 1 in classical applications, i.e. $M \in SL(2,\mathbb{Z})$.
We note that this is like a basis transformation of the paths, except that the monodromy matrix is unique (up to basis transformation) and is given by the system. As monodromy is a mixing of the paths, the monodromy matrix M not being the identity proves the presence of monodromy.

Following the paths, we remember to integrate the full inner product $\boldsymbol{p} \cdot d\boldsymbol{q}$, while this often reduces to integrating a single term for convenient paths. Since the integral is additive with respect to the paths, the integrals change in the same way after one turn:

$$\begin{pmatrix} I_1' \\ I_2' \end{pmatrix} = M \begin{pmatrix} I_1 \\ I_2 \end{pmatrix}.$$

The angles and frequencies transform according to $(M^{-1})^\dagger$ [11], following from the chain rule. The formula reads:

$$\begin{pmatrix} \omega_1' \\ \omega_2' \end{pmatrix} = (M^{-1})^\dagger \begin{pmatrix} \omega_1 \\ \omega_2 \end{pmatrix}.$$

In quantum physics, the deformation of the lattice cell is a linear transformation given by the monodromy matrix. It follows that the lattice cell is deformed only when moved along a path enclosing the singularity. An example of both cases is shown in Figure 2.7. We see that on the right the right edge is raised by one point while the remaining part remains intact. The matrix is then $M = \begin{pmatrix} 1 & 0 \\ 1 & 1 \end{pmatrix}$ in standard basis, and this way we can calculate monodromy matrices from spectra also later on. The integer condition on the monodromy matrix holds for a single unit cell, but may not hold for larger cells. As in an example in [13], we use a doubled moving cell and get $1/2$

[9] One cannot take just any two paths, they need to generate the first homology group of the torus. Hence these are called *fundamental paths*.

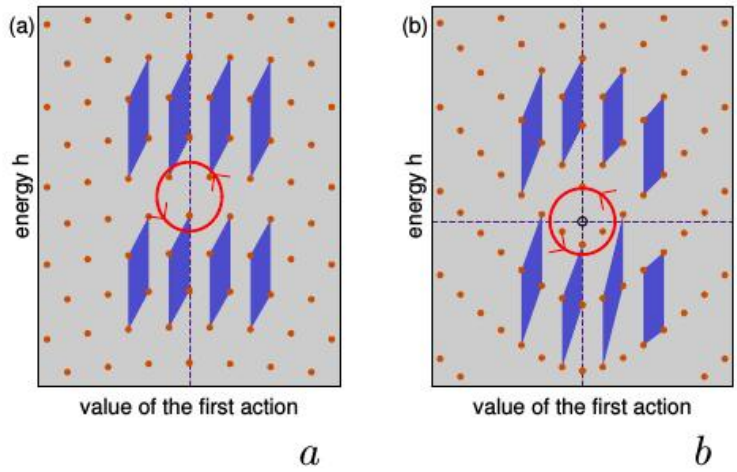

Figure 2.7: Monodromy and a quantum lattice [8]. On the left we see a cell transported in a normal lattice without singularity, and is not deformed. On the right, the lattice cell loops around the singularity marked by the dashed lines, and is clearly deformed. Note that the singularity does not need to be a point on the lattice(!).

in the matrix. The possible matrices are treated in more detail in [11].

We note that the monodromy matrix can also be calculated explicitly (as is done in [4]). The matrix is often filled by integers corresponding to the number of singular components (or just isolated singularites) enclosed by the path and depending on the chosen basis. Many more properties of the quantum lattice are described by the monodromy matrix, based on solid mathematics and semi-classical theory [11].

2.5 Examples of monodromy in physical systems

We would like to introduce two systems with monodromy to demonstrate its relevance in physics. First, we consider the spherical pendulum as a well-known system which is comparable to tri-atomic molecules (as e.g. used in [17]). Second, we see that a hydrogen atom in crossed electromagnetic fields exhibits monodromy.

Spherical Pendulum

We treat the spherical pendulum as an example, following [6]. We consider the phase space

$$P = \{(q,p) \in \mathbb{R}^3 \times \mathbb{R}^3 | < q,q >= 1, < q,p >= 0\}$$

where $< q,q >= 1$ makes sure that the position vector $q = (q_1, q_2, q_3)^T$ lies on the unit sphere, and $< q,p >= 0$ follows from taking the derivative of this relation. The energy

E and angular momentum L are given by

$$E = \frac{p^2}{2} + q_3$$
$$L = q_1 p_2 - q_2 p_1$$

and the standing up position is $q_3 = 1$, $q_1 = q_2 = p_1 = p_2 = p_3 = 0$ with corresponding $(L, E) = (0, 1)$. Taking the differentials of E and L gives that

$$dE = p_1 dp_1 + p_2 dp_2 + p_3 dp_3 + dq_3$$
$$dL = q_1 dp_2 + p_2 dq_1 - q_2 dp_1 - p_1 dq_2.$$

Hence $dL = 0$ and $dE = dq_3 = 0$ (from the restriction to the sphere) at the standing-up position, making them linearly dependent. So, we cannot appeal to Theorem 1 to conclude the existence of global *single-valued* smooth action-angle coordinates. Indeed, as pointed out in [6], the action functions generating the vector fields belonging to E and L are multi-valued.

The quantum spherical pendulum problem can be written with operators

$$\hat{H} = -\frac{\hbar^2}{2}\nabla^2 + z$$
$$\hat{L} = -i\hbar\left(x\frac{\partial}{\partial y} - y\frac{\partial}{\partial x}\right)$$

as $\hat{H}\psi = E\psi$, $\hat{L}\psi = L\psi$ where these operators work on states on the sphere.

One can then construct a 'quasiclassical spectrum' where $\hbar \to 0$. This spectrum shows monodromy in the sense that every real analytic function that is not a function of L alone and has level-curves passing through the quasiclassical spectrum (see Figure 2.8) cannot be single-valued. In [6], it is also argued that a basis lattice cell is deformed when passing around this spectrum. Physically, it means that when energy and angular momentum are varied smoothly to move around an obstruction, the change in configuration (relative position of states in the lattice) is not smooth.

We see that the deformation can be described by the matrix

$$\begin{pmatrix} 1 & 0 \\ 1 & 1 \end{pmatrix}$$

as the right edge is lifted by one point (similar to what we saw in the previous subsection). In general, we see monodromy matrices of the form

$$\begin{pmatrix} 1 & 0 \\ n & 1 \end{pmatrix}$$

where n is an integer measuring the number of singular components encircled. What does this mean physically? In any case it gives us the maximum number of locations (in

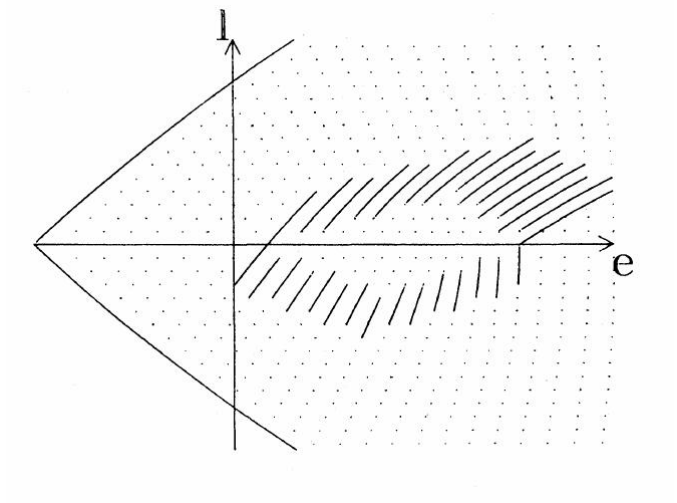

Figure 2.8: The quasiclassical spectrum from [6], where energy is on the horizontal axis and angular momentum on the vertical axis. The lines represent analytical functions needed for the transport of a lattice cell. That is, when we start on the right below the e axis, we move clockwise by jumping along the curves. We note that the lines then show that a usual square in the beginning is deformed.

EL-space) where our coordinate system will not be smooth. The precise distribution is not determined. In this case, the 1 originates from a single-pinched torus underneath the singularity (more details in [18]). In the following example we will have a 2, originating from a double-pinched torus underneath the singularity. However, encircling two isolated singularities both having a single-pinched torus will also give us $n = 2$. The difference is that we can have $n = 0, 1, 2$ by choosing our path appropriately (encircling none, one or two singularities resp.), while the double-pinched case only offers $n = 0, 2$.

Monodromy was at first not regarded as a physically relevant phenomena [8]. Later, people found monodromy in real systems. As an example, the hydrogen atom subjected to static orthogonal electric and magnetic fields exhibits monodromy.

Hydrogen atom in static, crossed electromagnetic fields

Following [19], when placing a hydrogen atom (proton plus electron) in a B-field in the x-direction and an E-field in the y-direction the Hamiltonian becomes (truncated and ignoring spin, relativistic effects and finite nuclear mass):

$$H = \underbrace{\frac{p^2}{2} - \frac{C}{|q|}}_{\text{Kinetic and potential part}} + \underbrace{Fq_2}_{\text{Stark effect}} + \underbrace{\frac{1}{2}G(q_2p_3 - q_3p_2) + \frac{1}{8}G^2(q_2^2 + q_3^2)}_{\text{Linear and quadratic Zeeman effect}}$$

where C represent the effective charge, F the electric field and G the magnetic field.

Using rescaling and perturbation theory, the eigenvalues of the operators can be calculated, giving the spectrum of Figure 2.9. This figure also shows a defect as a hollow circle and a lattice cell rotated clockwise, starting above the defect. This point was predicted by showing that the phase space becomes topologically a pinched torus. One can recognize an oval pattern in the lattice in the reddish shape, which follows from level curves (of certain invariants). These lines are used to transport points left-right (which involves also going up-down). For going purely up or down, we use the vertical arrangement of the points.

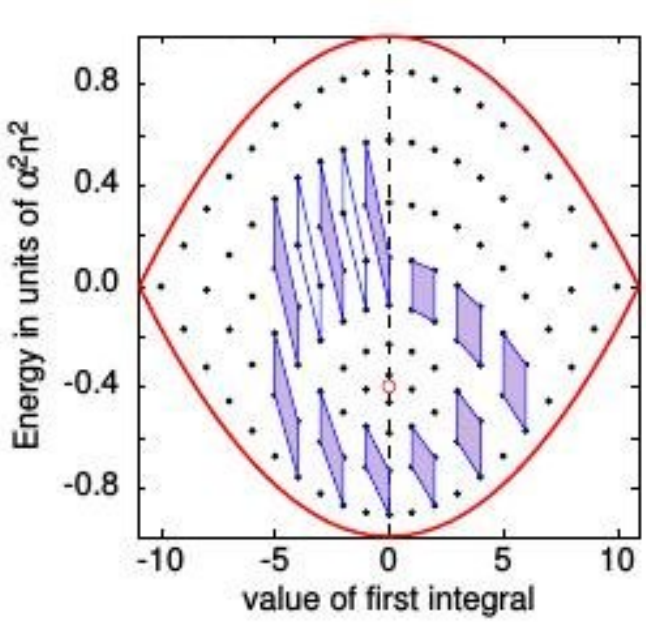

Figure 2.9: Spectrum of hydrogen atom subjected to static orthogonal electric and magnetic fields for an appropriately chosen field strength. Picture obtained from [8], original research in [19]

The first integral in this case is the average value of the linear perturbation of the (scaled) Hamiltonian, containing the linear terms of the electromagnetic-fields. We note that the picture depends on the magnetic field strength, and this was chosen conveniently to show monodromy.

Imagine that some way, it is physically possible to move from one state to the other (more in next subsection). The picture is fixed by the magnetic field, so the first integral (horizontal axis) can be varied alone by adjusting the electric field. The states for a given first integral differ by angular momentum quantum number, so the energy (vertical

axis) must e.g. be altered by emission/absorption of a photon. The rotation is then hypothetically performed in four steps;

1. The electron emits photons while the field is increased
2. The field is reduced to zero while the electron keeps emitting photons
3. The field is increased in the opposite direction and the electron absorbs photons
4. The field is again reduced and the electron absorbs photons

The figure then shows that a group of different states may return in a different configuration. This is not a precise set-up (nor is there any guarantee that this works), and we will discuss other possibilities in the next subsection.

The deformation of the cell can be expressed by the monodromy matrix M, i.e. M times the initial cell is the final cell. This matrix is

$$M = \begin{pmatrix} 1 & 2 \\ 0 & 1 \end{pmatrix}$$

where the 2 shows the monodromy. As said, if the matrix would be the identity, no monodromy occurs as the cell will remain intact.

2.6 Measuring monodromy

Theoretical approach

A question that remains is how to measure monodromy in an experiment involving in a system. Unfortunately, there is no straightforward method known in general; an experiment showing monodromy in this way is not found as far as we know.

Mathematical details of a possible experiment for a similar potential were discussed in [14]. Two main points of such an experiment are the way of traversing a closed loop around the singularity and what observations should be made. The paper argues that monodromy in a static system will result in non-trivial dynamical behavior in the same system with a well-chosen perturbation. To explain what this means, we resort to a closed loop in energy-momentum space. As both E and L are constant for the static Hamiltonian, letting particles move across the loop in time is impossible. Hence we need a perturbation to do this, but the question is then what kind of measurement we need to do. This can be done by following an *ensemble of particles*, and the observations consist of viewing the ensemble in configuration space and investigate its topological properties.

In the paper, it is shown that such perturbations exist, and the method is worked out for a Mexican hat potential $V \propto -r^2$ present in a disk, with infinite potential outside (as already discussed and seen in Figure 2.5). In Figure 2.10, we have a loop in energy-momentum space around the singularity, parametrized by an angle in minutes, and we

apply a perturbation which takes particles along this loop (so the angle also measures time). This introduces the dynamical part into the static system, and the measurement can be done as follows.

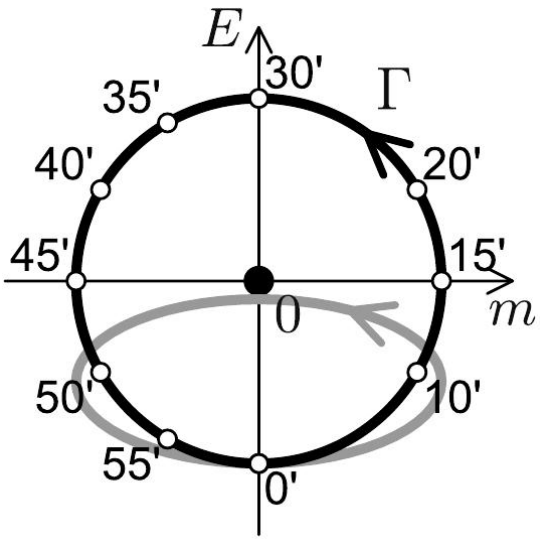

Figure 2.10: The loop showing how energy E and momentum m of the particles changes in time [14]. The loop in gray shows a loop under which the particles will not have non-trivial dynamical behavior.

We select an ensemble of (noninteracting) particles having the energy indicated by 0' and zero angular momentum. The available configurations are then radial motions climbing the hat, falling down on it to get specular reflected at the boundary and this repeats itself. This happens along a line, and we choose all our particles on one line on the right of the hat, see the first picture in Figure 2.11. So the red curve contains all possible configurations present in the line for the given energy and zero angular momentum. We then track our particles in time, which are influenced by the perturbation. We see that the particles will form their own loop, which itself also moves around the hat.

When we are at 30', or above the singularity with zero momentum but with energy higher then the barrier, the particles cross the origin. It is only for this moment that we have no forbidden region. The curve evolves further to enclose the region and remains so after we arrive back at our initial energy and angular momentum. So then, this perturbation makes us loop around the forbidden region. The gray loop in Figure 2.10 will not do such a thing. Since the calculations involved in this research are similar to these of the monodromy, the claim is that this topological alteration can be attributed to monodromy.

The next goal is to find an experimental set-up suitable. One candidate is the plane

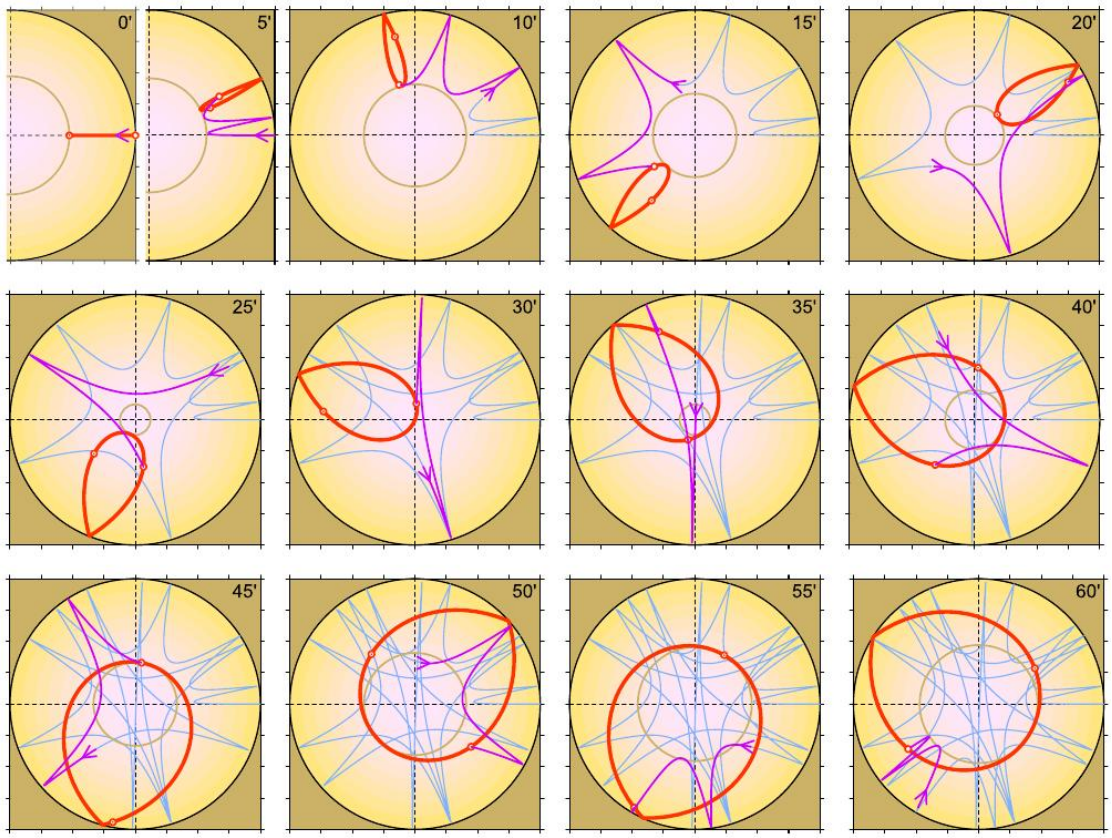

Figure 2.11: The particles in the disk with Mexican hat potential (red), tracked in time [14]. The yellow-brown circle in the middle shows the classically forbidden region. We see that after one turn, the projection has winded around this forbidden region.

switching[10] in carbondioxide, where already suitable energy levels were investigated in [20]. Using polarized laser light one could influence the resonant swing motion. Circular polarized light then affects the momentum, and linear polarized light mainly the energy. Combining the knowledge of these findings may result into an appropriate perturbation using the laser light, which is able to change the topological distribution of an ensemble of particles in a non-trivial way.

Measurements in other systems

Another way to see monodromy by means of an experiment is to measure the spectrum. Naturally, one can use the moving cell method, but also the shapes/lines formed by similar states will show different behavior depending on their location w.r.t. the singularity. See Figure 2.12 for example. The lines emphasize the change in behavior after passing

[10]This effect consists of an abrupt change in the energy balance between stretching modes and swinging modes of the molecule.

a value close to 11100cm^{-1}, which corresponds to the energy barrier for linear geometry of the molecule. That way, we have a singularity in a similar manner as the spherical pendulum.

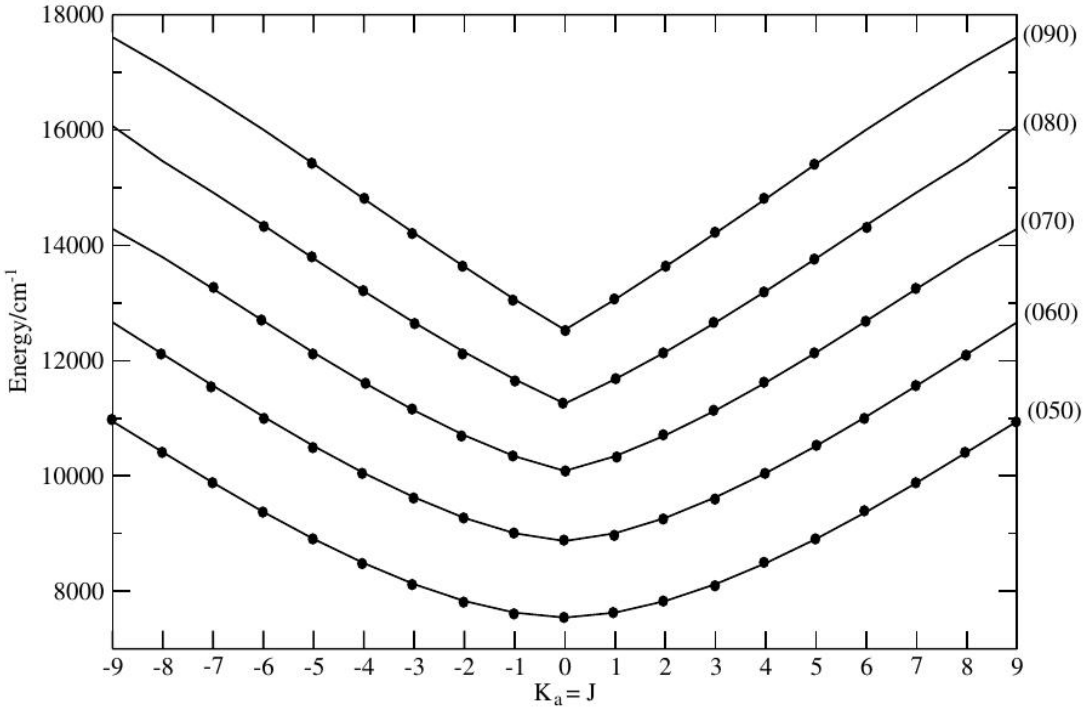

Figure 2.12: Selected rotational level bands of the water molecule [12]. The lines connect states of the same degree of bending excitation (marked by frequencies $\nu_1\nu_2\nu_3$ on the right). The stretching modes are not excited ($\nu_1 = \nu_3 = 0$).

The way this pictures hints to monodromy is like the argument in Figure 2.6. If there is monodromy, we will not be able to connect states in a smooth way. To really show monodromy, one could use a moving cell or analyse a model for the system.

3 The radial square-well with barrier

In this section we investigate the system given by a circularly symmetric square-well with additional barrier. We first consider the configuration and materials themselves, to then solve the classical and quantum equations.

3.1 The quantum system

In the macroscopic world classical mechanics is used to describe the world. This is possible because the length scales exceed by many orders of magnitude the (de Broglie) wavelengths of individual particles. It is at the scale of these waves that quantization conditions change the behavior of the system dramatically. One of the systems with this appropriate dimension is a so-called quantum dot (sometimes called nano-crystal, but that is a broader concept). It usually consists of a 'dot' of specific shape of semiconductor material. In quantum dots [21], the charge carriers (electrons and holes) are confined by potential barriers to these small regions and form the main subject of study to deduce the properties of the dot. Typical length scales at which quantum effects begin to occur in semiconductors is about 20nm. A quantum dot confines all three spatial directions. It is also possible to confine a system in only two directions, which is named a quantum wire (or quantum rod). If we confine only one direction, so that we have planar system, we have a so-called quantum well (or quantum film).

We will investigate a system with a potential as follows. Outside a planar disk of radius R (=1 if we scale our units) the potential is infinite. This disk is split using a centered circle of radius R_1 where the potential has constant value V_0. The remaining region has potential 0. So we have:

$$V(r) = \begin{cases} V_0 & \text{if } r < R_1 \\ 0 & \text{if } R_1 < r < 1 \\ \infty & \text{if } r > 1 \end{cases}$$

This system, as in Figure 3.1, is like an (idealized) two dimensional material (graphene for example) where a barrier can be created by the electric field effect using a thin insulator or by local chemical doping [22]. We have to make additional assumptions for the realization. We assume that particles feel the potential difference (and so not fly through by the Klein paradox). Also, we will be using the usual Schrödinger equation instead of Dirac equation, which is not completely appropriate for graphene because of its lattice structure. Another way of realizing this system may be with two rings of different (semiconductor) material, where electrons would feel two different potentials (so one may need other two dimensional materials).

To create quantum dots, various ways are available. One can directly deposit vapor (molecular beam epitaxy (MBE) or metallo-organic chemical vapor deposition (MOCVD))

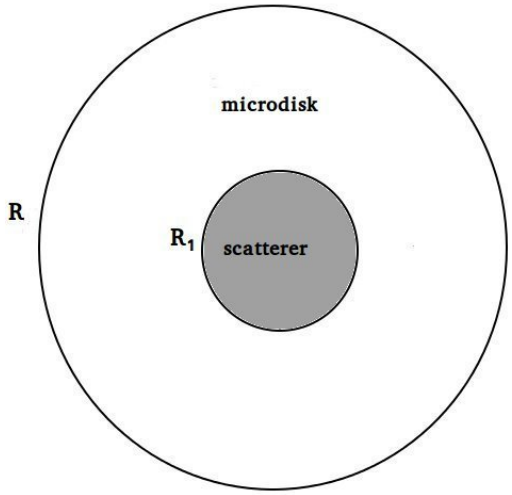

Figure 3.1: A schematical picture of the microdisk with scatterer.

or use chemical synthesis (colloidal chemistry or electrochemistry). Implementing quantum dots in already existing devices can significantly improve performance and this has attracted attention. An example is to use quantum dots to improve the conversion of photons into electron-hole pairs in solar cells. Another advantage is that one can still use inexpensive materials as basis, but get a higher efficiency (even higher than thermodynamic limits).

The idea of this procedure came up in the late 1970s, and early in the 1980s the first specifically synthesized quantum dots to investigate quantization by size were made. Nanocrystals were already used in e.g. stained glass, but the quantum effects were not recognized until the 1970s. Examples of early reported materials are CdS, CdSe, CdTe, InP, GaAs and GaP. In the years following, many aspects of quantum dots and nanocrystals could be controlled better. The reaction temperatures decreased, the size and shape could be made closer to the desired ones and surface chemistry had improved.

Applications of nanocrystals and quantum dots are increasing in number. Also neuroscience is looking into them; [23] uses them in combination with fluorescence microscopy as quantum dots combined small size with high optical resolution. They could also aid in medicine as photosensitizers [24], where exciting the quantum dot causes another molecule to have a reaction and so one can locally supply the medicine (which is the basis of photodynamic therapy). Also information processing techniques can be made using quantum dots as qubits [21, 25, 26].

When the system (and hence the potential) is circular symmetric, the wave-function usually has a trivial angular part and a potential-specific radial part. The angular part gives rise to allowed modes, and in combination with the radial part defines the allowed

energies.

It is comparable to a hydrogen atom with angular momentum $\hbar\sqrt{l(l+1)}$ and energy $E_n(eV) = -13.6/n^2$ where $l = 0, 1, \ldots, (n-1)$. This gives a lattice as discussed in Section 2.3 on quantum monodromy. We note that this is not a confined two dimensional system, but the interpretation and construction of the spectrum are similar.

We will know continue with a classical interpretation of the system.

3.2 Phase portrait of classical analogue

Taking the angular repulsion into account, the potential we must use is:

$$V_{\text{eff}}(m, r) = \begin{cases} m^2/r^2 + V_0 & \text{if } 0 \leq r < R_1 \\ m^2/r^2 & \text{if } R_1 < r < 1 \\ \infty & \text{if } r > 1 \end{cases}$$

The difference is illustrated in Figure 3.2, where we set $R_1 = 0.5$ and $V_0 = 300$ from now on.

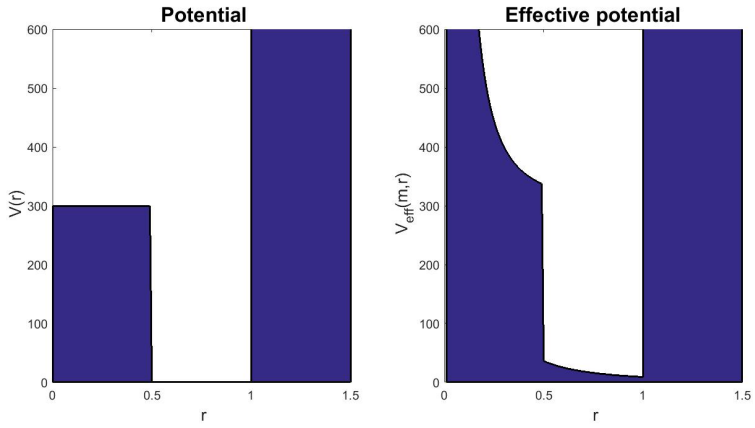

Figure 3.2: Visualization of the potential and the effective potential (for $m \neq 0$). The effective potential is not piecewise constant, and we will see these three different regions many times in calculations.

Then, we can obtain the phase portrait for the system by plotting

$$p_r(m, r) = \pm\sqrt{2(E - V_{\text{eff}}(m, r))}$$

versus r. We can fix the energy E and vary m, and the other way around. If we fix the energy and let m run from 0 to 12 in steps of 4, we get Figure 3.3a.

As expected, in the first figure $E < V_0$, and so the solution is only inside the well. We note that the solution seizes to exist if m is increased beyond a certain threshold.

The other pictures have $E \geq V_0$ and they indeed show pieces inside the whole allowed region. Here, only the $m = 0$ states reach $r = 0$ since only then the potential does not blow up. Fixing m and varying E above and below V_0 gives Figure 3.3b.

In both pictures, we see states that can be connected continuously (i.e. connecting the positive and negative branch of the momentum) and those which cannot. Physically, imagine a particle entering on the right side with negative momentum, that is, towards the center. At some point, the particle must move away from the center, which means that the momentum must become positive. If the curve in the phase portrait is connected, the orbit will turn in a continuous way. If it is not connected, the particle bounces off the barrier. Looking at the potential, we see that if $m \neq 0$ the solution is not connected if $m^2/R_1^2 < E < m^2/R_1^2 + V_0$. On the other hand, if $m = 0$, we see no solution can be connected (except the one where $E = V_0$, but then we have zero velocity inside the barrier). Here we see a special position for $m = 0$.

The most likely candidate for monodromy is an isolated singularity. This occurs at the axis $m = 0$ since there the bifurcation occurs, in the way that then phase portraits consist of piecewise constant functions only, which does not happen for $m \neq 0$. The energy value of the singularity is the height of the potential barrier of the inner region for $m = 0$, i.e. V_0. Also, the pre-image of this point under the energy-momentum map $\mathcal{EM}$ is not a well-defined torus. The modes flying around the inner disk form no problem, but every location inside the disk implies zero velocity, pinching the phase space (so the set of (q, p) looks like a pinched torus). Other orbits include particles getting stuck on the edge of this region.

We can check if we fulfill the requirements of the Liouville-Arnold theorem. Since we have 2 integrals (l and E) in involution, we must show that they are dependent for $E = V_0$ and $l = 0$.

In polar coordinates (r, θ), implying conjugate momenta (p_r, p_θ), the relations are:

$$\begin{aligned} E &= \frac{1}{2m}\left(p_r^2 + \frac{p_\theta^2}{r^2}\right) + V(r) \\ l &= p_\theta. \end{aligned}$$

Then $l = 0$ implies for the differentials

$$\begin{aligned} dE &= \frac{1}{m} p_r dp_r + V_0 \delta(R_1 - r) dr \\ dl &= dp_\theta. \end{aligned}$$

For a particle inside the inner disk, $p_r = 0$, and so $dE = 0$, meaning dependency. For a particle outside, $p_r = \sqrt{2mV_0}$, so dE and dl are independent. However, we thus see that the differentials are not independent on the whole level set. This means that the point $(l, E) = (0, V_0)$ is a singularity. So indeed, we cannot appeal to Theorem 1 to have appropriate action-angle coordinates.

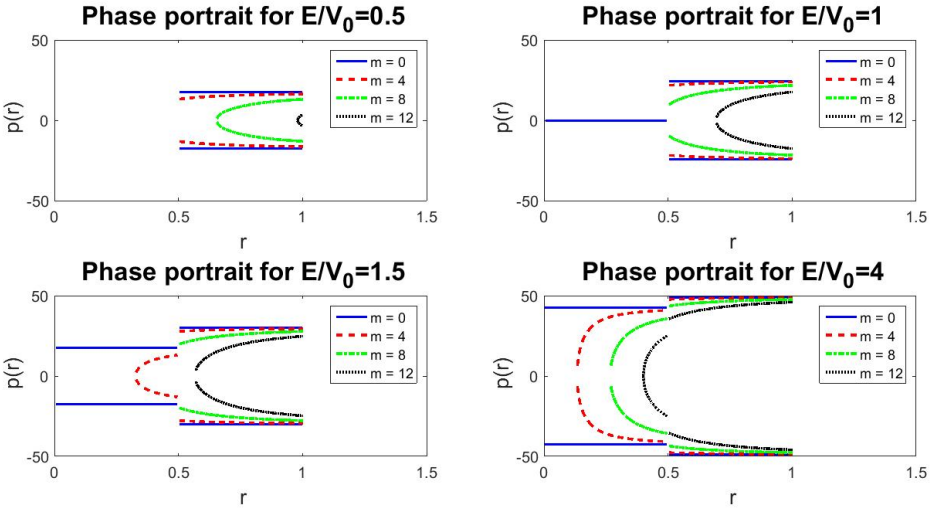

(a) Phase portraits for fixed energy.

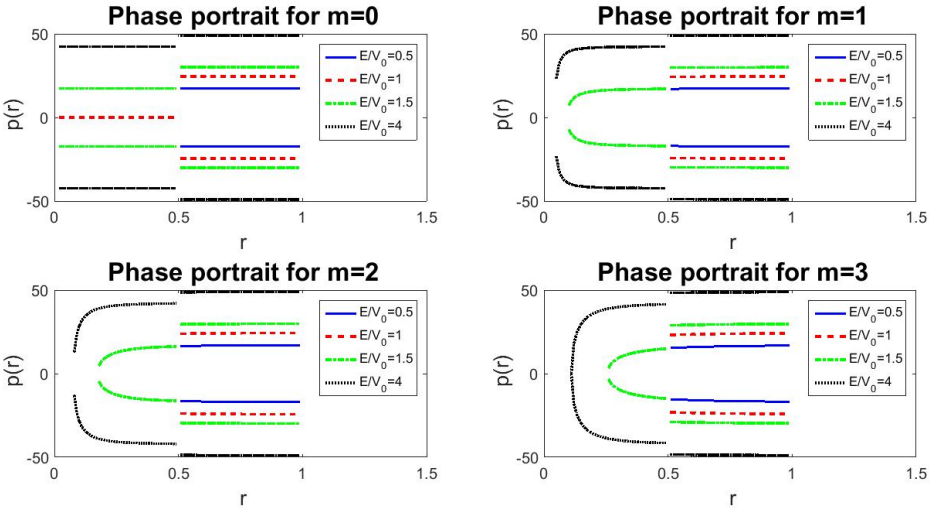

(b) Phase portraits for fixed m. Note the difference between energies above and below V_0.

Figure 3.3: Phase portrait given by the billiard system.

3.3 Billiard motion

In this subsection we continue with the classical analogue of a particle (electron) bouncing around in the potential with specular (ideal elastic) reflection at the boundary. This motion is described using a billiard map, which maps one reflection to the next. The calculation of this map can be found in Appendix A. In this section, we will use this map to investigate its properties and construct its action-angle coordinates.

In Figure 3.4, various billiard motions are shown, made using the billiard map. We

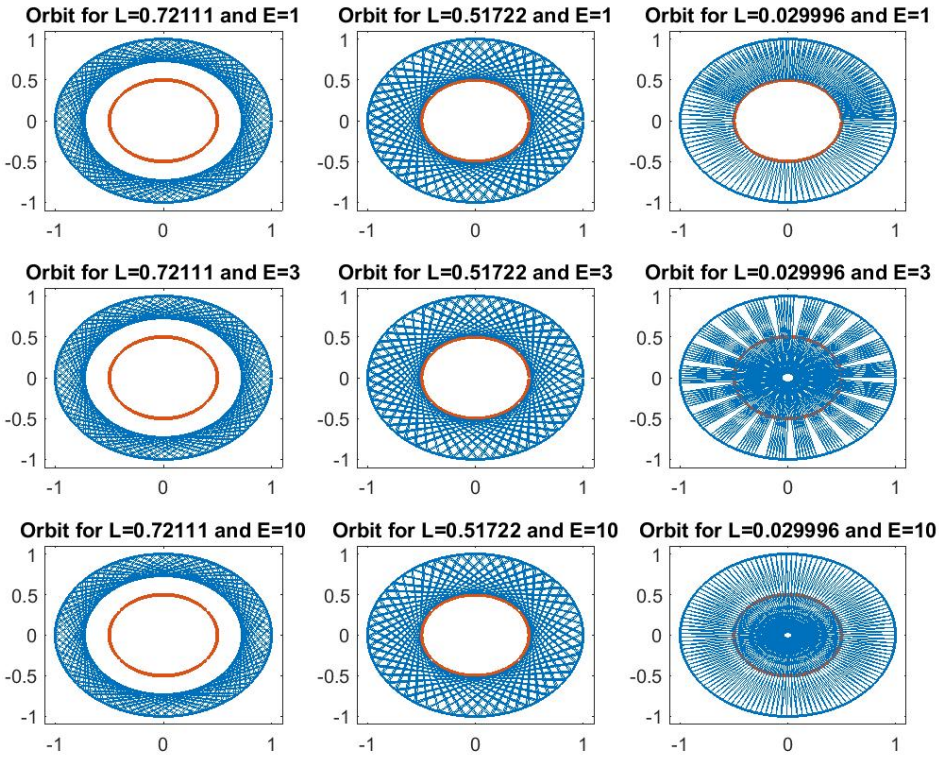

Figure 3.4: Billiard motion for different values of angular momentum l and the energy E, where in each case $V_0 = 2$.

see basically three different motion, as we could deduce from the three regions of the effective potential. On the left, angular momentum is so large that the particle moves along the boundary. This motion is called a *whispering gallery mode* (or WGM), after its acoustical equivalent. These modes disappear when angular momentum is decreased. In the middle, we can see reflection of the particle by the inner disk in this energy range. On the right, angular momentum is so small that the particle can penetrate the inner disk (if E is high enough), but is refracted by conservation on angular momentum. We

will call this motion hence refraction.

If we let s measure the arc-length of the outer circle and ϕ the angle the particle makes with the positive tangent. We recognize that the billiard map is an endomorphism, mapping a cylinder to itself. Since ϕ (and so $\cos(\phi)$) are conserved, orbits will be points on straight lines in a s, ϕ-diagram, which are thus invariant lines (see Figure 3.5). These lines have periodic points depending on the chosen ϕ. The lines at $\phi = \pm\pi/3$ are made up of points with period 3 (triangle-shaped orbit), filling the whole line if we vary s. When the (constant) variation of s is irrational, we will find no periodic orbit. This picture will not depend much on the energy; the orbits may be deformed, but will still add up to a continuum. We can clearly recognize reflection turning into refraction as the dense orbits in the middle spread out. This change starts when E/V_0 passes the value 1, and the area in which the effect is apparent grows with this ratio.

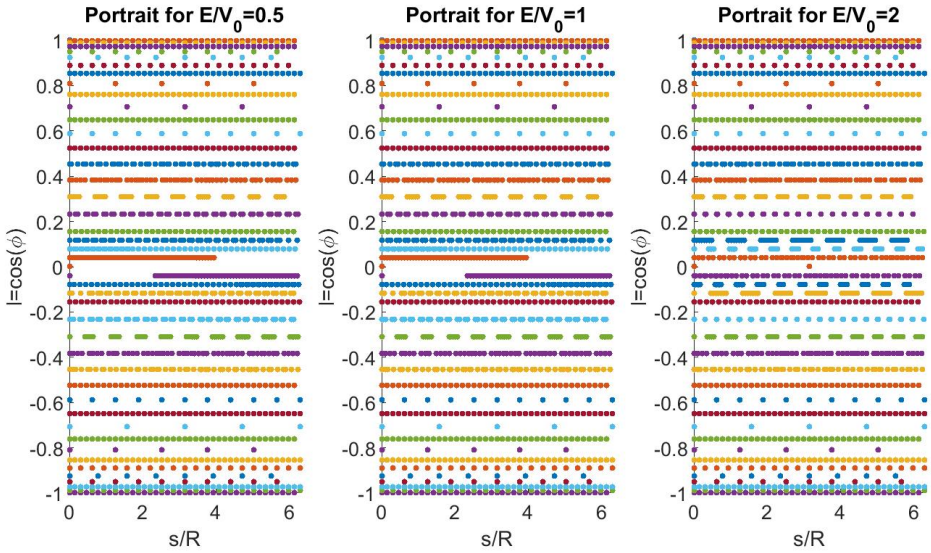

Figure 3.5: Phase plots of the billiard map. For various angles, 50 iterations for the orbit starting at $s = 0$ are shown. We see a bifurcation when E exceeds V_0.

Having seen all these billiard motions, we can relate them to the monodromy picture. We repeat that the singularity is situated at zero momentum with energy V_0. For other values of the momentum (we omit 'angular' as we only use this momentum for the rest of this section) with the same energy, it is not possible to be inside the inner disk (since the momentum should vanish, giving a contradiction). For other energies, and in general, other pre-images contain billiard motion consisting of reflection (and refraction). The possibility of reaching the center is exclusively for $l = 0$ and staying there only for $E = V_0$.

Modifications of the annular billiard exist, such as a displacement of the inner disk such that the circles are no longer concentric. This also means that the billiard map will

now have non-trivial invariant lines, see [27]. Depending on the non-concentricity, most invariant lines will have vanished.

Action-angle variables in the billiard

The actions are defined as

$$\begin{aligned} I_1 &= \frac{1}{2\pi}\oint_{\gamma_1} p_r dr \\ I_2 &= \frac{1}{2\pi}\oint_{\gamma_2} p_\phi d\phi \end{aligned} \tag{3.1}$$

where we already used some properties of the paths. For γ_1, a natural choice is the cycle consisting of moving from the outer boundary and back (which corresponds to the orbit captured by one iteration of the billiard map), and so we only have to integrate $p_r dr$. As γ_2, we picked the motion of performing one turn around the center, and so we only integrate the other term of the inner product. Hence, the second is easily solved by noting that $p_\phi = l$ is a constant of motion:

$$I_2 = \frac{1}{2\pi}\oint_{\gamma_2} l d\phi = \frac{1}{2\pi}(2\pi l) = l.$$

The first integral is defined piecewise, depending on the energy, since the turning points (the integration limits) do so. We consider three regions, depending where and how the particle hits the inner disk. Considering Figure 3.2, we can hit the steep wall or get smoothly repelled if the energy is either high or low enough. There is no reflection by the inner disk if $E < l^2/(2mR_1^2)$ or $E > V_0 + l^2/(2mR_1^2)$, which we call region 1 and region 3 respectively. The energies that are left form region 2, where we are specularly reflected by the inner disk. For convenience, we will rewrite p_r and these energy conditions in the new units. Since $\frac{1}{2m}\left(p_r^2 + \frac{l^2}{r^2}\right) + V = E$, we have

$$p_r = \sqrt{2m(E-V) - \frac{l^2}{r^2}} = \sqrt{2mE}\sqrt{1 - \frac{V}{E} - \frac{l^2}{2mEr^2}}.$$

Scaling $\sqrt{2mE} = 1$, so $m = (2E)^{-1}$, we can simplify to

$$p_r = \sqrt{1 - \frac{V}{E} - \frac{l^2}{r^2}}.$$

The condition $E < l^2/(2mR_1^2)$ turns out to be

$$E < E\frac{l^2}{R_1^2} \implies 1 < \frac{l^2}{R_1^2}$$

and the second becomes

$$E > V_0 + E\frac{l^2}{R_1^2} \implies 1 > \frac{V_0}{E} + \frac{l^2}{R_1^2}.$$

In region 1, we have $V = 0$ and the turning points are $r = R = 1$ and $r = |l|/\sqrt{2mE} = |l|$. So, keeping in mind that a cycle consists of both back and forth motion between these points, the action becomes:

$$(I_1)^1 = \frac{1}{\pi}\int_{|l|}^{1}\sqrt{1-\frac{l^2}{r^2}}dr = \frac{1}{\pi}\left(\sqrt{1-l^2}+|l|\tan^{-1}\left(\frac{|l|}{\sqrt{1-l^2}}\right)\right)-\frac{|l|}{2}. \tag{3.2}$$

The second region is similar, only the inner turning point is now fixed at $r = R_1$. In this case, the formula is

$$\begin{aligned}(I_1)^2 = \frac{1}{\pi}\int_{R_1}^{1}\sqrt{1-\frac{l^2}{r^2}}dr = \frac{1}{\pi}\Bigg(&\sqrt{1-l^2}+|l|\tan^{-1}\left(\frac{|l|}{\sqrt{1-l^2}}\right)\\ &-\sqrt{R_1^2-l^2}-|l|\tan^{-1}\left(\frac{|l|}{\sqrt{R_1^2-l^2}}\right)\Bigg).\end{aligned} \tag{3.3}$$

The last case is where the particle penetrates the disk up to a distance

$$r_0 = \frac{|l|}{\sqrt{1-V_0/E}} < R_1.$$

The potential knows two regions, so we have to calculate the integral piecewise:

$$(I_1)^3 = \frac{1}{\pi}\left(\int_{r_0}^{R_1}\sqrt{1-\frac{V_0}{E}-\frac{l^2}{r^2}}dr+\int_{R_1}^{1}\sqrt{1-\frac{l^2}{r^2}}dr\right).$$

We can copy the right integral from the previous case, and only need to calculate the first. This new contribution equals

$$\frac{1}{\pi}\left(\sqrt{\left(1-\frac{V_0}{E}\right)R_1^2-l^2}+|l|\cot^{-1}\left(\sqrt{\left(1-\frac{V_0}{E}\right)R_1^2-l^2}\right)\right)-\frac{|l|}{2}$$

and so the action equals

$$\begin{aligned}(I_1)^3 =&\frac{1}{\pi}\left(\sqrt{\left(1-\frac{V_0}{E}\right)R_1^2-l^2}+|l|\tan^{-1}\left(\frac{|l|}{\sqrt{\left(1-\frac{V_0}{E}\right)R_1^2-l^2}}\right)\right)-\frac{|l|}{2}\\ &+\frac{1}{\pi}\left(\sqrt{1-l^2}+|l|\tan^{-1}\left(\frac{|l|}{\sqrt{1-l^2}}\right)-\sqrt{R_1^2-l^2}-|l|\tan^{-1}\left(\frac{|l|}{\sqrt{R_1^2-l^2}}\right)\right).\end{aligned} \tag{3.4}$$

Summarizing, the action I_1 is given by Equations (3.2) to (3.4) according to:

$$I_1(l,E) = \begin{cases} (I_1)^1(l,E) & \text{if } 1 < \dfrac{l^2}{R_1^2} \\ (I_1)^2(l,E) & \text{if } \dfrac{l^2}{R_1^2} < 1 < \dfrac{V_0}{E} + \dfrac{l^2}{R_1^2} \\ (I_1)^3(l,E) & \text{if } 1 > \dfrac{V_0}{E} + \dfrac{l^2}{R_1^2} \end{cases} \tag{3.5}$$

where the domain consists of all non-negative energies E and $|l| \leq 1$ by the scaling. How this domain is divided over the regions can be seen in Figure 3.6.

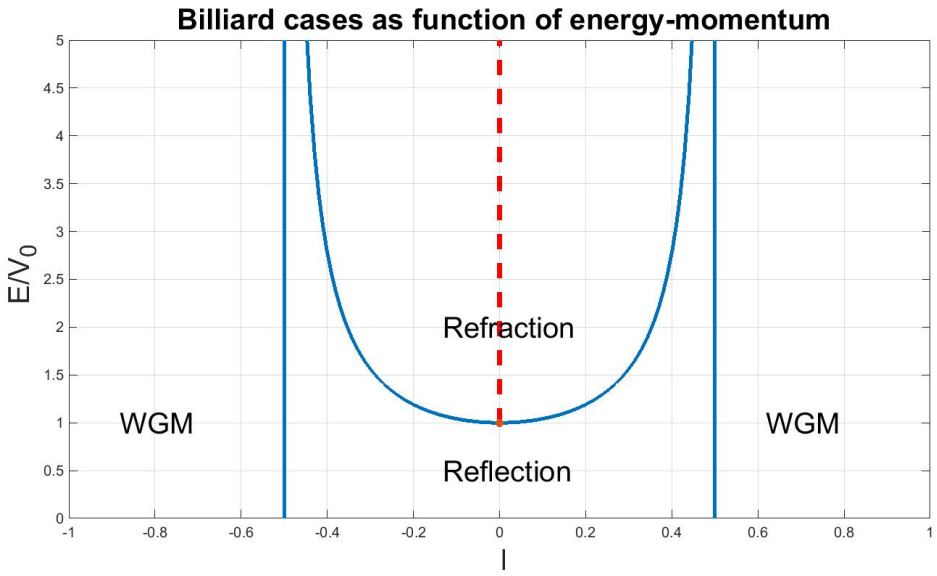

Figure 3.6: Cases of the billiard map and action I_1 distributed over energy-momentum space. The vertical lines are situated at $|l| = R_1$, and the other lines asymptotically approach these. The dashed line in red will be important later when we discuss the smoothness of the action I_1.

A quick evaluation of the limits $|l| \to R_1$ and $|l| \to R_1\sqrt{1 - V_0/E}$ (keeping E constant) shows that the action is continuous. A graph of I_1 versus l for various energies can be found in Figure 3.7, where we remember that I_1 is measured in units of $R\sqrt{2mE}$. We note that the action is bounded. As p_r is maximal for $V_0/E = 0$, $l = 0$ and the limits are between 0 and $R = 1$, we can see

$$I_1 \leq \frac{1}{\pi}\int_0^1 \sqrt{1}dr = \frac{1}{\pi} \approx 0.318.$$

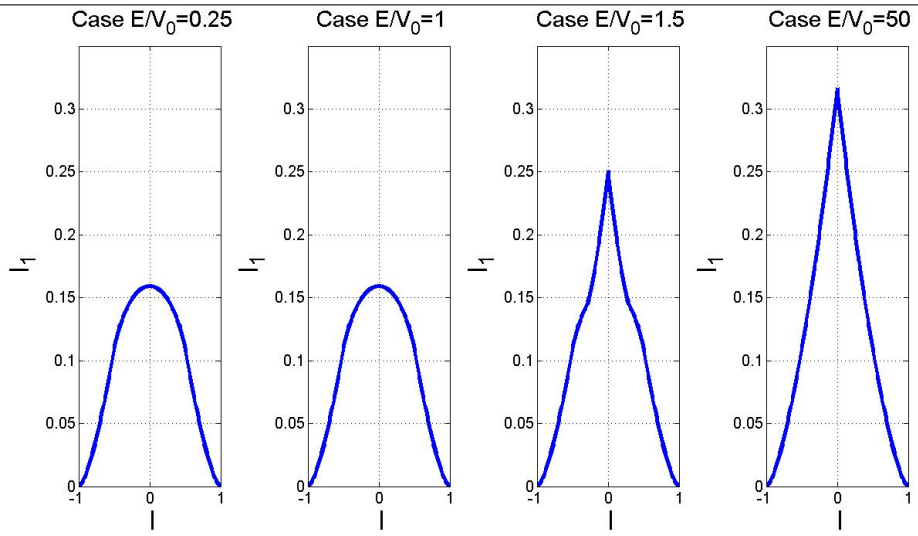

Figure 3.7: Graph of the action I_1 versus the momentum l for various values of the energy.

We would now like to follow the ratio of the radial frequency and the angular frequency, where these frequencies are defined according to Definition 2.3. This reduces then to the winding number as in Equation (2.2), and implementing $I_2 = l$, we see

$$W := \frac{\omega_2}{\omega_1} = -\frac{\partial I_1}{\partial l}. \tag{3.6}$$

Hence, the next step is to calculate the partial derivative with respect to l and change its sign. The derivative was evaluated numerically and is shown in Figure 3.9a.

Immediately, we see that the graph contains sharp edges, meaning that this action is *not smooth*. This however does not prove monodromy, since we only showed that this particular choice of fundamental paths produces an action that is not smooth and single-valued globally. A transformation as described in Section 2.4 allows us to follow the winding number in a smooth way. Since we have no trouble with l, we can keep it as we like; $l' = l$. We see that the winding number suddenly increases by 1. So, we can make it smooth by adding $-l$ to I_1 for $l < 0$. Letting this new action be I_1', the equation becomes[11]:

$$\begin{pmatrix} I_1' \\ l' \end{pmatrix} = \begin{pmatrix} 1 & -1 \\ 0 & 1 \end{pmatrix} \begin{pmatrix} I_1 \\ l \end{pmatrix}.$$

Not coincidently, this matrix was already seen when inspecting the spectrum (Equation (3.12) on page 40).

[11] Maybe the fact that the number is negative inside the matrix is odd considering that it represents the number of singular components. This can be reconciled in many ways. One can use a basis transformation (then the number changes sign and moves to below-left), or, one can instead of subtracting l add it to the other side, (making the number only change sign).

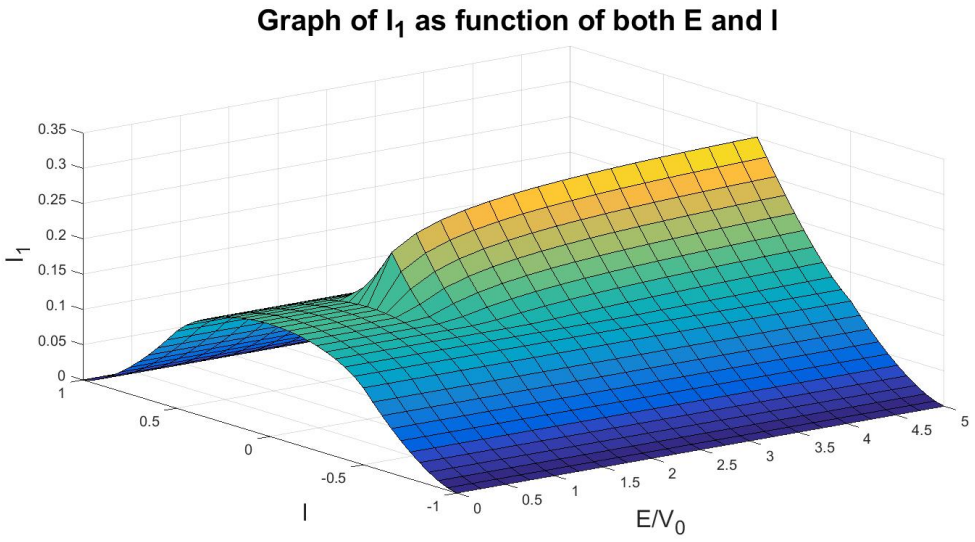

(a) A surf plot of I_1.

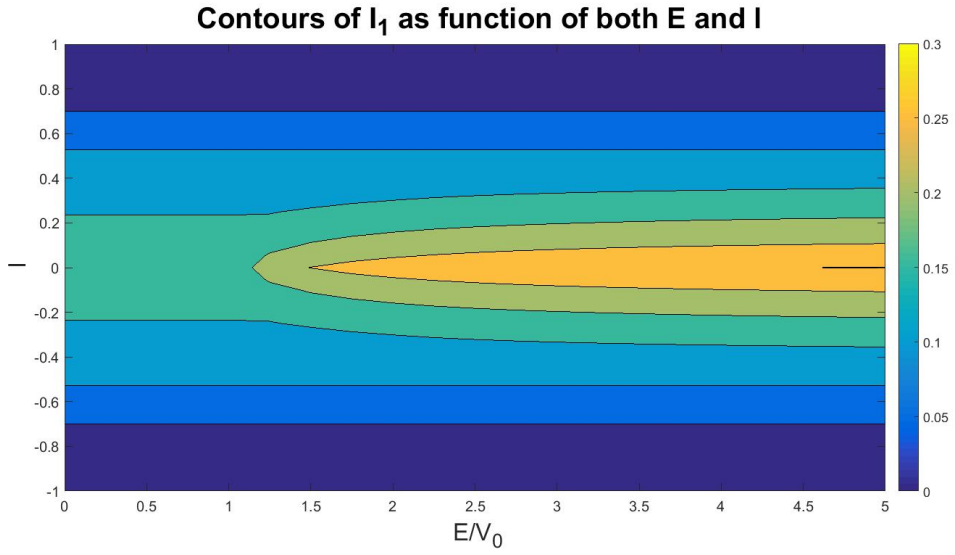

(b) A contour plot of I_1.

Figure 3.8: Two different plots showing the action I_1 as function of both l and E.

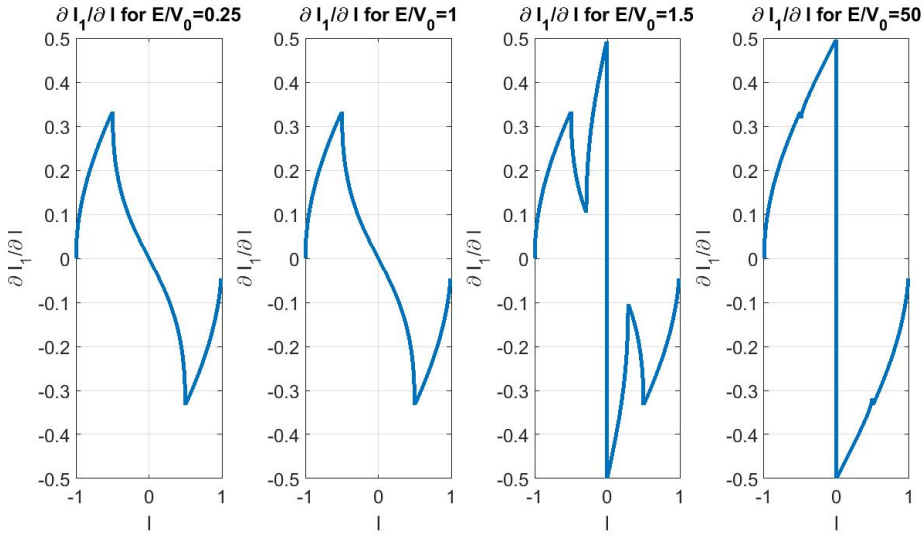

(a) Plot of the partial derivative of I_1 with respect to l.

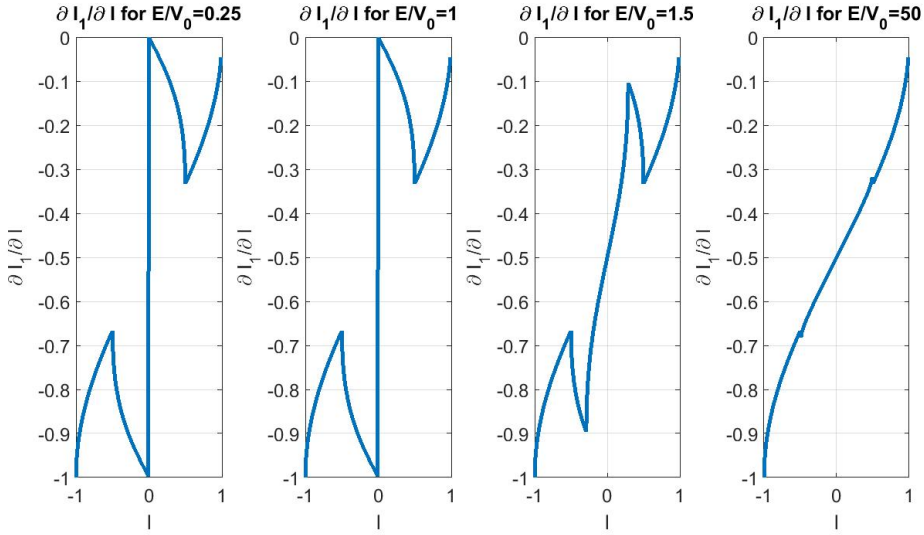

(b) The derivative after smoothing around $l = 0$ for the region $E > V_0$.

Figure 3.9: Plots of the partial derivative of I_1 w.r.t. l. We see that the smoothness is exchanged between the regions $E \leq V_0$ and $E > V_0$.

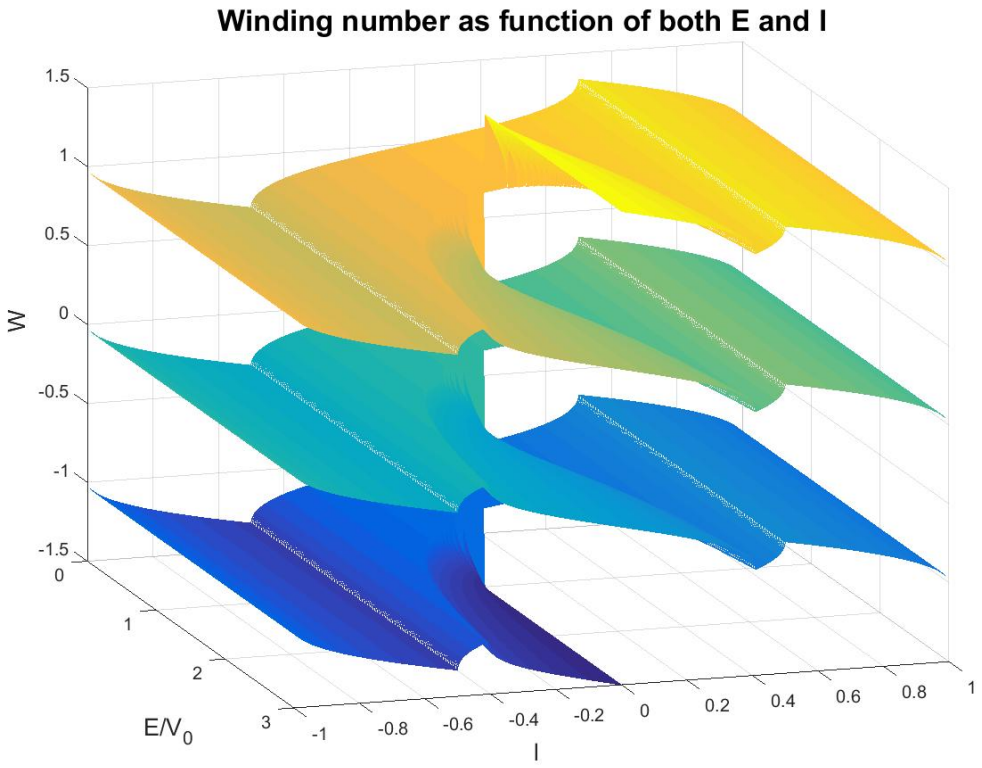

Figure 3.10: Surface obtained by imposing smooth winding number in a neighborhood of the singularity.

Consider any closed loop around the singularity. Take a starting point (l_0, E_0) not on the line $l = 0$. When traversing the path up to the half-line upward from the singularity, our winding number (or derivative) is smooth and we need no different choice in actions (so the matrix is the identity and thus not affecting further calculations). When traversing this half-line, say we travel in positive direction (counterclockwise), we have to switch over to $I_1' = I_1 + l$. But when we arrive back at (l_0, E_0), we have the values $I_1(l_0, E_0)$ and $I_1'(l_0, E_0) = I_1(l_0, E_0) - l_0$ which differ by $l_0 \neq 0$. Hence, if we have smooth and globally defined action-angle coordinates, they cannot be single-valued. This proves rigorously that the system exhibits monodromy. As a final illustration of this effect, see Figure 3.10, where the surface is shown if we insist on tracking the winding number smoothly in a closed loop close to the origin. We can clearly see how multi-valuedness is crucial to this procedure.

3.4 The spectrum

In this section, we will calculate the spectrum analytically and by approximating it using the WKB method. The methods produce similar spectra, and both of these show monodromy using the moving cell method.

Direct approach

The time-independent Schrödinger equation $H\Psi = E\Psi$ under the assumption that the z-component plays no role reduces to the equation

$$-\frac{\hbar^2}{2\mu}\left(\frac{\partial^2\Psi}{\partial r^2}+\frac{1}{r}\frac{\partial\Psi}{\partial r}+\frac{1}{r^2}\frac{\partial^2\Psi}{\partial\phi^2}\right)+V\Psi=E\Psi. \tag{3.7}$$

If the system is rotationally symmetric, so that the potential depends only on r, we can separate variables using the ansatz $\Psi(r,\phi)=\psi(r)\Phi(\phi)$. The equation becomes

$$r^2\frac{\psi''}{\psi}+r\frac{\psi'}{\psi}+r^2\frac{2\mu}{\hbar^2}(E-V)=-\frac{\Phi''}{\Phi}=m^2 \tag{3.8}$$

where the left part depends only on r, the middle part only on ϕ and the right part m^2 is our separation constant. The angular part gives then

$$\Phi''=-m^2\Phi \implies \Phi(\phi)=c_1e^{im\phi}+c_2e^{-im\phi}.$$

By imposing $\Phi(\phi+2\pi)=\Phi(\phi)$, it follows that m is an integer.

Using the obtained relation, we see

$$r^2\frac{\partial^2\psi}{\partial r^2}+r\frac{\partial\psi}{\partial r}+\left(\frac{2\mu}{\hbar^2}(E-V)r^2-m^2\right)\psi=0. \tag{3.9}$$

Changing variables to $x=\sqrt{\frac{2\mu}{\hbar^2}(E-V)}r$ transforms the equation to

$$x^2\frac{\partial^2\psi}{\partial x^2}+x\frac{\partial\psi}{\partial x}+\left(x^2-m^2\right)\psi=0. \tag{3.10}$$

The solutions to Equation (3.10) are the Bessel functions. Two linearly independent solutions are J_m and Y_m, named Bessel function of the first and second kind respectively. A special feature of J_m is that it is regular at 0.

We have three domains with 2 boundaries. Using appropriate boundary conditions, and scaling units such that $\frac{2m}{\hbar^2}=1$, the solutions are:

$$\Psi_m=\begin{cases}A_mJ_m(\sqrt{E-V_0}r)e^{\pm im\phi} & \text{if } r<R_1\\ [B_mJ_m(\sqrt{E}r)+C_mY_m(\sqrt{E}r)]e^{\pm im\phi} & \text{if } R_1<r<1\\ 0 & \text{if } r>1\end{cases}$$

The coefficients A_m, B_m, C_m represent the amplitudes. The solution usually is a linear combination of two independent solutions, like the solution for the middle part. Our boundary conditions impose us to pick a special linear combination for the first part. That is, we need a regular function at 0, since infinite values at the center are physically unrealistic. As described, we then pick J_m for the first since this is the only combination that is regular at the origin. It is obvious that the wave-function is zero in the region with infinite potential.

We require the wave-function and its radial derivative to be continuous at the boundary at $r = R_1$, which gives us two equations:

$$\begin{aligned} A_m J_m(\sqrt{E - V_0}R_1) &= B_m J_m(\sqrt{E}R_1) + C_m Y_m(\sqrt{E}R_1) \\ \sqrt{E - V_0}A_m J'_m(\sqrt{E - V_0}R_1) &= \sqrt{E}B_m J'_m(\sqrt{E}R_1) + \sqrt{E}C_m Y'_m(\sqrt{E}R_1). \end{aligned}$$

At the boundary at $r = R$ we require only continuity, so the wave function must vanish there. As said, if we measure distance in units of R, we scale it away to 1 and get:

$$B_m J_m(\sqrt{E}) + C_m Y_m(\sqrt{E}) = 0.$$

These equations can be summarized in a homogeneous matrix equation:

$$\begin{pmatrix} J_m(\sqrt{E - V_0}R_1) & -J_m(\sqrt{E}R_1) & -Y_m(\sqrt{E}R_1) \\ \sqrt{E - V_0}J'_m(\sqrt{E - V_0}R_1) & -\sqrt{E}J'_m(\sqrt{E}R_1) & -\sqrt{E}Y'_m(\sqrt{E}R_1) \\ 0 & J_m(\sqrt{E}) & Y_m(\sqrt{E}) \end{pmatrix} \begin{pmatrix} A_m \\ B_m \\ C_m \end{pmatrix} = \begin{pmatrix} 0 \\ 0 \\ 0 \end{pmatrix}.$$

The existence of an eigenstate requires a non-trivial solution of this system, and so we must set the determinant of the matrix equal to zero. This condition can be written as

$$\begin{aligned} &J_m(\sqrt{E})[\sqrt{E - V_0}Y_m(\sqrt{E}R_1)J'_m(\sqrt{E - V_0}R_1) - \sqrt{E}J_m(\sqrt{E - V_0}R_1)Y'_m(\sqrt{E}R_1)] \\ &- Y_m(\sqrt{E})[\sqrt{E - V_0}J_m(\sqrt{E}R_1)J'_m(\sqrt{E - V_0}R_1) - \sqrt{E}J_m(\sqrt{E - V_0}R_1)J'_m(\sqrt{E}R_1)] \\ &= 0 \end{aligned}$$

and using $J'_m(z) = J_{m-1}(z) - \frac{m}{z}J_m(z)$ (from [28]) we can work out the algebra to remove the derivative (effectively by lowering the corresponding index by 1):

$$\begin{aligned} &J_m(\sqrt{E})\big[\sqrt{E - V_0}Y_m(\sqrt{E}R_1)J_{m-1}(\sqrt{E - V_0}R_1) \\ &\quad - \sqrt{E}J_m(\sqrt{E - V_0}R_1)Y_{m-1}(\sqrt{E}R_1)\big] \\ &- Y_m(\sqrt{E})\big[\sqrt{E - V_0}J_m(\sqrt{E}R_1)J_{m-1}(\sqrt{E - V_0}R_1) \\ &\quad - \sqrt{E}J_m(\sqrt{E - V_0}R_1)J_{m-1}(\sqrt{E}R_1)\big] \\ &= 0 \end{aligned} \tag{3.11}$$

So, when an integer value for m is picked, we can (numerically) solve Equation (3.11) to get a spectrum of E values. Notice that in the derivation leading to m (Equation (3.8))

we in fact encounter m^2 instead of m, that is, the direction of angular momentum is irrelevant. Hence the E values found for m are the same as for $-m$. This means that if $m \neq 0$, the E values are double degenerate (assuming that for different $|m|$ we get different energies). By the same reasoning; if $m = 0$, then the E values are nondegenerate.

We want to solve the equation numerically using a Newton procedure. This is a well-known way of numerically solving equations, and needs good initial guesses (especially because we have multiple zeros). To get these, we start first by ignoring the V_0 barrier, so we assume $R_1 = 0$ at first. The condition reduces then to $J_m(\sqrt{E}) = 0$, so we need (the square of) the roots of a Bessel function, which can be found easily. Then we increase R_1 from zero to a chosen value slowly. Each time we increase it, we run the Newton procedure to 'keep track of the resonances'. Adjusting R_1 in the right way will then give us the solution for the real system.

We note that it is no longer possible to scale V_0 away as we already took $R = 1$ and $\frac{2\mu}{\hbar^2} = 1$. The first sets a length scale, and since the second fixed a conversion between length and energy, also the energy scale is fixed. Implementing $V_0 = 300$ and $R_1 = 0.25$ as arbitrary values produces the spectrum in Figure 3.11a. We mark the singularity by an open circle.

To show that monodromy is present, we use the method of the moving unit cell. We move using the locally defined structure, that is by adjusting m to go sideways and straight up and down to complete the turn. The result of this is found in Figure 3.12a.

Inspecting the deformation of the lattice cell for a clockwise oriented loop around the singularity, we see that the deformation is captured by the matrix

$$\begin{pmatrix} 1 & -1 \\ 0 & 1 \end{pmatrix} \tag{3.12}$$

since the points are now lowered. Going the other way will raise another edge, the matrix for a counterclockwise turn is:

$$\begin{pmatrix} 1 & 0 \\ 1 & 1 \end{pmatrix}.$$

As pointed out in [11], these matrices are equivalent and differ only by a basis transformation (they are each others inverse transposed). We see the integer appearing now in another space, but this also follows from a basis transformation.

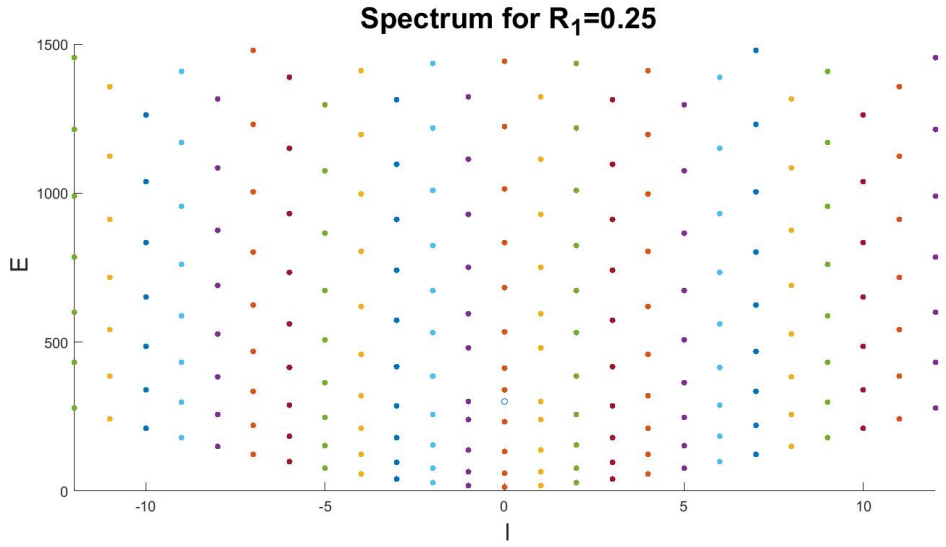

(a) Spectrum for $R_1 = 0.25$.

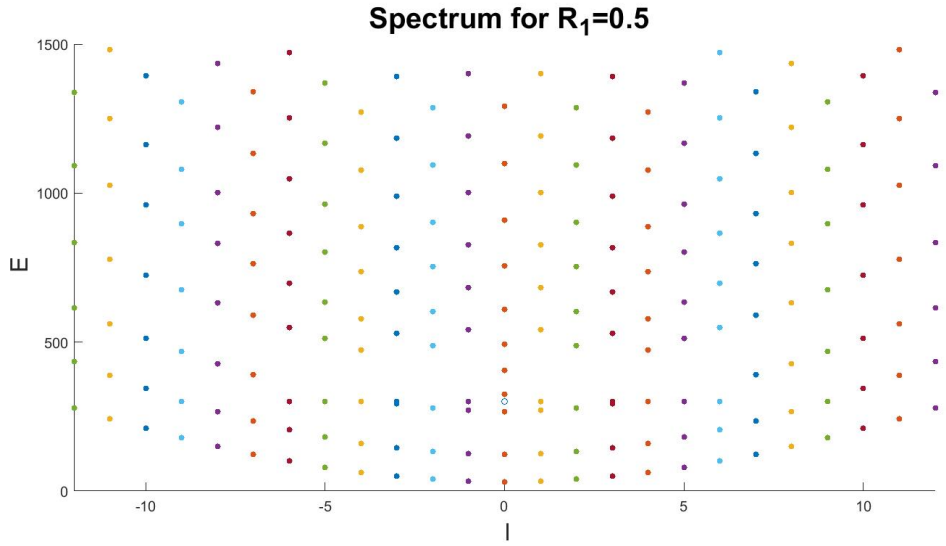

(b) Spectrum for $R_1 = 0.5$.

Figure 3.11: Spectra given by the resonance condition. The singularity $(0, V_0) = (0, 300)$ is marked by a hollow dot.

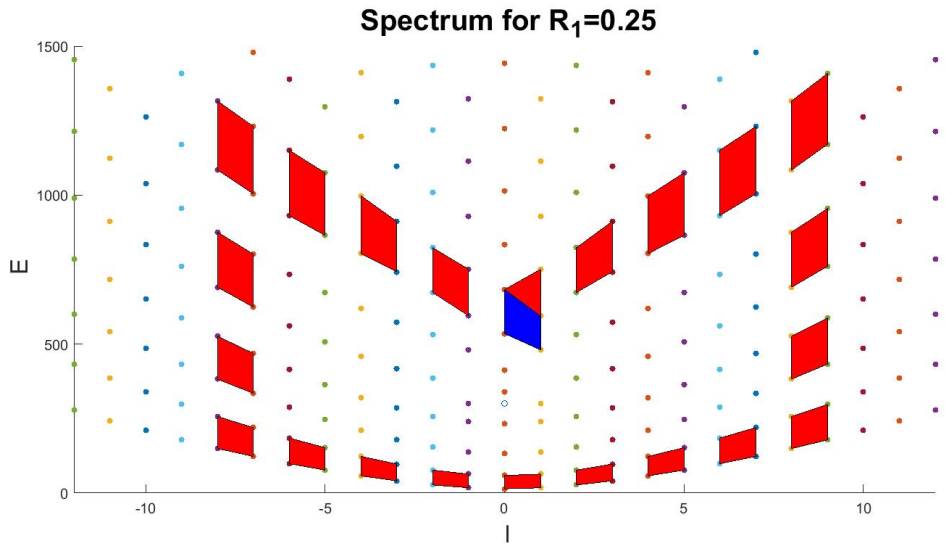

(a) Moving cell in the case $R_1 = 0.25$.

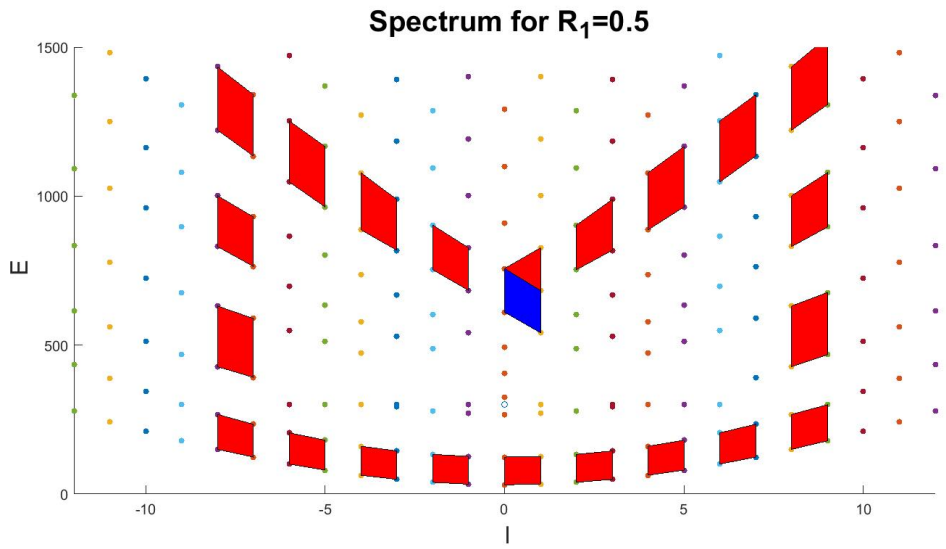

(b) Moving cell in the spectrum for $R_1 = 0.5$.

Figure 3.12: The distortion of a cell moving around the singularity. Starting in the middle above the singularity and moving clockwise, we indeed return with another shape of the lattice cell.

The WKB method

Quantum physics knows many approximation methods, one of which is the WKB method. We will briefly introduce its concepts and formulas. We will see that it uses a semi-classical approach, and is thus very useful in the context of this thesis.

The Schrödinger equation

$$-\frac{\hbar^2}{2\mu}\frac{d^2\psi}{dx^2} + V(x)\psi = E\psi$$

can be rewritten using a classical definition for momentum. If we define

$$p(x) = \sqrt{2\mu(E - V(x))},$$

the equation becomes

$$\frac{d^2\psi}{dx^2} = -\frac{p^2}{\hbar^2}\psi. \tag{3.13}$$

If we use the ansatz $\psi(x) = e^{if(x)/\hbar}$, we find that

$$i\hbar f'' - (f')^2 + p^2 = 0.$$

Writing $f(x) = f_0(x) + \hbar f_1(x) + \hbar^2 f_2(x) + \dots$ and collecting powers of $\hbar$, we find for $\hbar^0$ and $\hbar^1$ respectively:

$$\begin{aligned}(f_0')^2 &= p^2\\ if_0'' &= 2f_0'f_1'.\end{aligned}$$

We see

$$f_0'(x) = \pm p \implies f_0(x) = \pm\int p(x)dx$$

$$f_1'(x) = \frac{if_0''}{2f_0'} = \frac{ip'}{2p} = \frac{i}{2}\frac{d}{dx}\ln(|p|) \implies f_1(x) = \frac{i}{2}\ln(|p|) + c.$$

So if we approximate the wave-function up to first order in $\hbar$, we find that

$$\begin{aligned}\psi(x) = e^{if(x)/\hbar} &\approx e^{\frac{i}{\hbar}(\pm\int p(x)dx + \hbar\frac{i}{2}\ln(|p|)+c)}\\ &= e^{-\frac{1}{2}\ln(|p|)+c'}e^{\pm\frac{i}{\hbar}\int p(x)dx} = \frac{C}{\sqrt{|p(x)|}}e^{\pm\frac{i}{\hbar}\int p(x)dx}\end{aligned}$$

where the general solution is a linear combination of the + and - solutions and C is a phase. Another way to derive these equations is to use the ansatz $\psi(x) = A(x)e^{i\phi(x)}$ where $A(x), \phi(x)$ (amplitude and phase) are some *real* functions. A derivation is given in [29]. Since the method is classically motivated and is the actual wave-function up to first order in $\hbar$, the method is called semi-classical. It works well when $A''(x)/A(x)$ is

much less than both $(p(x)/\hbar)^2$ and $(\phi'(x))^2$

We implicitly assumed $E > V(x)$, but $E < V(x)$ works fine too provided that the exponent gets an extra i, because p is now imaginary, which then gives exponential decay.

The problems left are the turning points where $E \approx V(x)$ such that $p(x) \approx 0$ and the pre-factor blows up. This is solved by gluing the wave-functions together with a locally defined new wave-function. In a small enough neighborhood the potential is approximately linear, and plugging this into the Schrödinger equation shows that we need Airy functions. Matching the functions together gives rise to *connection formulas* relating the coefficients of the independent solutions. An important consequence is a phase alteration between adjacent parts of the approximate wave-function by $\pm\pi/4$, where the sign depends on the orientation.

Now that we have all this, we can use WKB to approximate the energies. For convenience we write the linear combination in sine and cosine using $\phi(x) = \frac{1}{\hbar}\int p(x)dx$:

$$\psi = \frac{1}{\sqrt{p(x)}}(c_1 \sin(\phi(x)) + c_2 \cos(\phi(x)).$$

Consider a square-well extending from 0 to a. Then we know $\psi(0) = \psi(a) = 0$. From $\psi(0) = 0$, we see $c_2 = 0$, and then $\psi(a) = 0$ shows us that $\phi(x) = \frac{1}{\hbar}\int p(x)dx = n\pi$. So, to get the energy for states between infinite potential walls, one solves

$$\int p(x)dx = n\pi\hbar$$

for E (which enters via p).

If we consider also the connection formulas in the argument above, the formula to get the energy yields

$$\int p(x)dx = (n - k/4)\pi\hbar \tag{3.14}$$

where k is the number of non-vertical potential sides, and the turning point is assumed to be on the right side of the classically allowed region $E > V(x)$.

Applying WKB

Since the original potential is piecewise constant and varies little with angular repulsion, we hope that the WKB method gives a good approximation. We treat three cases separately; $E < m^2/R_1^2$, $m^2/R_1^2 < E < V_0 + m^2/R_1^2$ and $E > V_0 + m^2/R_1^2$.

In the case $E < m^2/R_1^2$, we have a turning point at

$$r_1 = \frac{|m|}{\sqrt{E}}$$

and so the condition becomes

$$\int_{r_1}^{1} \sqrt{E - m^2/r^2}dr = \sqrt{E - m^2} + |m| \tan^{-1}\left(\frac{|m|}{\sqrt{E - m^2}}\right) - \frac{|m|\pi}{2} = \left(n - \frac{1}{4}\right)\pi. \quad (3.15)$$

For $m^2/R_1^2 < E < V_0 + m^2/R_1^2$, we have an infinite barrier at $r = 1$, but the barrier at $r = R_1$ is not infinite. Hence the quantization condition becomes

$$\int_{R_1}^{1} \sqrt{2\mu(E - m^2/r^2)}dr = \left(n - \frac{1}{4}\right)\pi\hbar$$

or in rescaled units

$$\int_{R_1}^{1} \sqrt{E - m^2/r^2}dr = \left(n - \frac{1}{4}\right)\pi.$$

The solution is

$$\begin{aligned} &\sqrt{E - m^2} + |m| \tan^{-1}\left(\frac{|m|}{\sqrt{E - m^2}}\right) \\ &\quad - R_1\sqrt{E - m^2/R_1^2} - |m| \tan^{-1}\left(\frac{|m|}{\sqrt{ER_1^2 - m^2}}\right) = \left(n - \frac{1}{4}\right)\pi \end{aligned} \quad (3.16)$$

where n is such that the energy does not exceed V_0. The case $m = 0$ is special, and the energy is easily found to be

$$E_n = \frac{\left(n - \frac{1}{4}\right)^2 \pi^2}{(1 - R_1)^2}. \quad (3.17)$$

For the case $E > V_0$, we again have a infinite barrier at $r = 1$, but the left barrier depends on m. For $m = 0$, we can get to $r = 0$, which we can see as an infinite potential wall. The condition is then

$$\int_0^{R_1} \sqrt{E - V_0}dr + \int_{R_1}^{1} \sqrt{E}dr = n\pi.$$

or

$$\sqrt{E - V_0} + u\sqrt{E} = n\pi/R_1 \quad (3.18)$$

where $u = (1 - R_1)/R_1$. If $R_1 = 0.5$ or $u = 1$, the equation can be solved to give

$$E = \frac{E_n}{4} + \frac{V_0}{2} + \frac{V_0^2}{4E_n}$$

where $E_n = n^2\pi^2\hbar^2/2\mu R_1^2 = n^2\pi^2/R_1^2$ and we require $E > V_0$ so that we have a condition on n.

If now $m \neq 0$, we see a classical turning point where $E = V$ in the region of the barrier. In this case we have $V = V_0 + m^2/r^2$, indeed implying that the turning point depends on m. If r_0 describes the turning point, it is given by

$$r_0 = \frac{|m|}{\sqrt{E - V_0}}.$$

Hence we see that the turning point occurs where the potential is again not an infinite wall. Thus, the quantization condition reads

$$\int_{r_0}^{R_1} \sqrt{E - V_0 - m^2/r^2}dr + \int_{R_1}^{1} \sqrt{E - m^2/r^2}dr = \left(n - \frac{1}{4}\right)\pi$$

and evaluating the integral shows us

$$\begin{aligned} &R_1\sqrt{E - V_0 - m^2/R_1^2} + |m|\tan^{-1}\left(\frac{|m|}{R_1\sqrt{E - V_0 - m^2/R_1^2}}\right) - \frac{|m|\pi}{2} \\ &\quad + \sqrt{E - m^2} + |m|\tan^{-1}\left(\frac{|m|}{\sqrt{E - m^2}}\right) - R_1\sqrt{E - m^2/R_1^2} \\ &\quad - |m|\tan^{-1}\left(\frac{|m|}{R_1\sqrt{E - m^2/R_1^2}}\right) \\ &= \left(n - \frac{1}{4}\right)\pi. \end{aligned} \tag{3.19}$$

Equations (3.15) to (3.19) provide the energies predicted by the WKB method. The equations together produce the whole spectrum, picking only the roots in the predetermined domain. Using numerical methods when necessary, we get a spectrum shown in Figure 3.13a.

We see the spectrum resembles Figure 3.11a resulting from the exact equation. The fact that we used different cases concerning energy is apparent around the singularity where some points are closer together and so form a gap underneath.

To check for monodromy, we again move a lattice cell around. The loop is less smooth, as seen in Figure 3.13b. Nevertheless, we still see that monodromy is present.

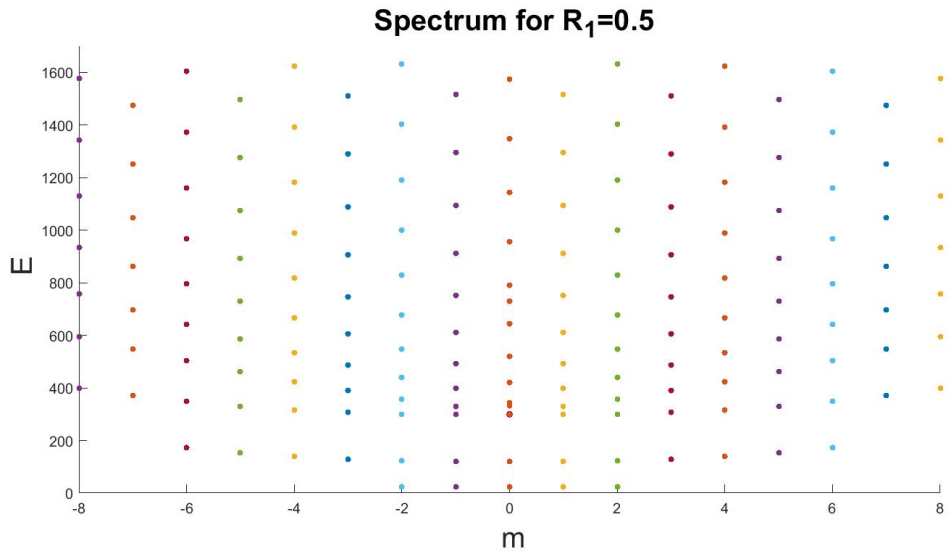

(a) The spectrum obtained using the WKB method.

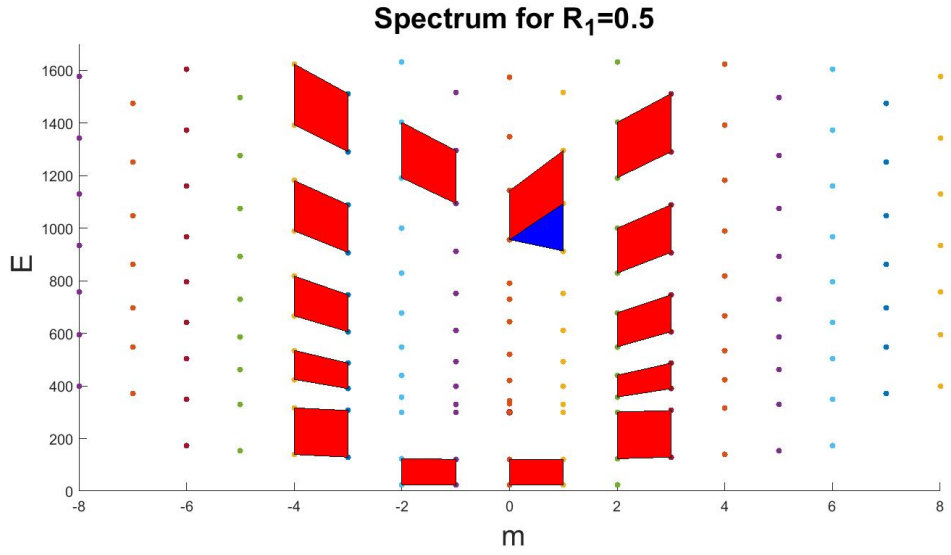

(b) Moving a cell in the spectrum obtained using the WKB method.

Figure 3.13: The spectra and moving cell in the WKB case.

4 Optical Microresonator

In this section, we will introduce optical microresonators. This was our original motivation to investigate monodromy, and we note that these system would be very suitable for a 'closed loop perturbation' experiment. However, as we will see, the potential corresponding to these systems will make it almost impossible for monodromy to exist. The material will be divided into three sections. Firstly, we will introduce the microresonators, and secondly derive the equation describing the wave-function. Finally, we will look at the classical analogue of the system and discuss conditions for monodromy to be present.

4.1 Introduction to optical microresonators

A broad introduction to concepts and uses of microcavities was given in Nature [30], and we will adapt some of the information to give an introduction. Optical microresonators are miniature cavities in which light can be trapped for long time. The micro scale is important, since the size will determine the resonance spectrum. The lines should hence be more sparsely distributed in comparison with a larger 'macro' resonator. An ideal resonator would trap light for infinite time, but in practice this is still impossible. The crucial parameters of a device are its volume (V) and the trapping time measured in optical periods (Q), which characterizes the deviation from an ideal resonator. The microresonators appear in many shapes, and an example of a circular resonator is given in Figure 4.1

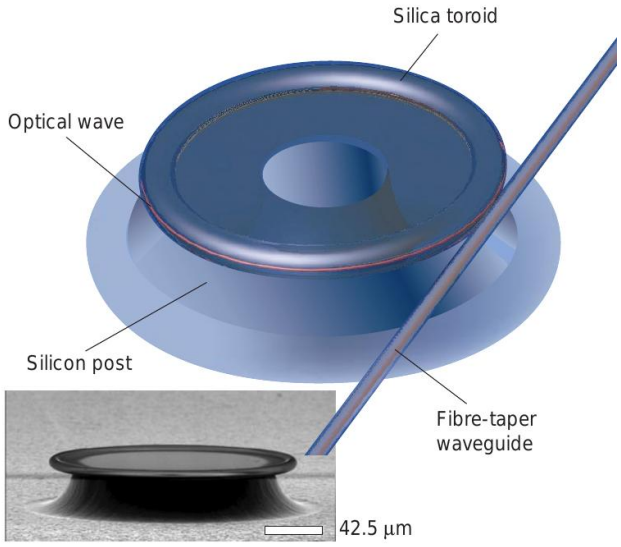

Figure 4.1: Illustration of a microtoroid, where the disk is used to trap a wave coupled to a fiber-taper waveguide [30].

Optical microresonators can be used in various applications including strong-coupling cavity quantum electrodynamics (QED), enhancement and suppression of spontaneous emission, dynamic filters in optical communication and as laser sources [30]. The applications arises from different properties of the resonator.

QED uses the possibility of letting an atom/molecule interact coherently with a cavity mode. The atom/molecule will then split the transmission spectrum according to the new-formed entangled states. This effect can hence be used to determine the position of cold molecules.

To enhance/suppress spontaneous emission one uses the fact that modes of the resonator are quasi-modes and not really stationary. The adjustment uses the Purcell effect; the rate of spontaneous emission depends on the density of final states ('Fermi's golden rule', [31]), which depend on the size and quality of the resonator. The quasi-modes can then be used as available states, in other words, they form lower energy states available for atoms having higher energy, allowing these atoms to decay under emission.

The dynamic filters can be realized by changing the refractive index electronically, and so changing the resonance frequencies. In long-distance communication, wavelength division not only provides a larger bandwidth by providing a larger number of channels, it can also improve performance. That is, if it is no longer needed to convert light to an electronic signal, much time can be won [32]. This method can only be implemented by having rapidly changing optical filters.

Microcavities can also be used as laser sources. For this, we consider [33] a practically flat disk, or a circle of a dielectric material (embedded in material with lower refractive index). Also Figure 4.1 gave an illustration of the schematic lay-out. The principle used is total internal reflection, so when light hits the boundary with an angle of at least the critical angle θ_c (measured w.r.t. the normal of the surface). This depends on the refractive index n of the material by the relation $\sin\theta_c = 1/n$. Using the circular symmetry, the light may travel along a billiard path along the boundary of the circle; the whispering gallery modes. These modes trap light for considerable time. For example, the disk in Figure 4.1 has $Q > 10^8$ (while the diameter is in the range of some 100μm). These modes can be used in a laser setting, where the wave can get out as an evanescent wave[12] [34].

The procedure has the disadvantage that light is emitted isotropically, and so one can't focus the light. This can be solved by breaking the symmetry of the circular dielectric microresonator to have light in particular directions. One way of doing this is to turn the circle into an ellipse, and the new intensity pattern is visualized in Figure 4.2a.

The particular system we wanted to look at was a microresonator with a scatterer inside. Physically, one could do this by placing a metal inside. Scatterers can be used for directional emission (also in circular symmetric resonator) while retaining the high Q-factor [35]. An illustration of this principle is found in Figure 4.2b. However, we

[12] An evanescent wave appears in the wave-equations to satisfy the continuity boundary conditions. These solutions in quantum mechanics correspond to the wave tunneling out.

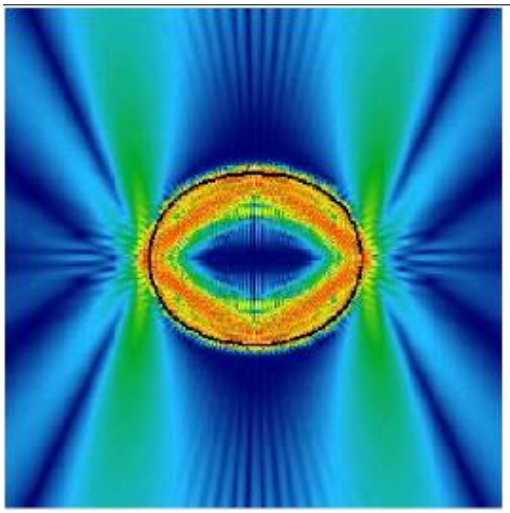

(a) The intensity pattern for an ellipsoidal dielectric microresonator [33].

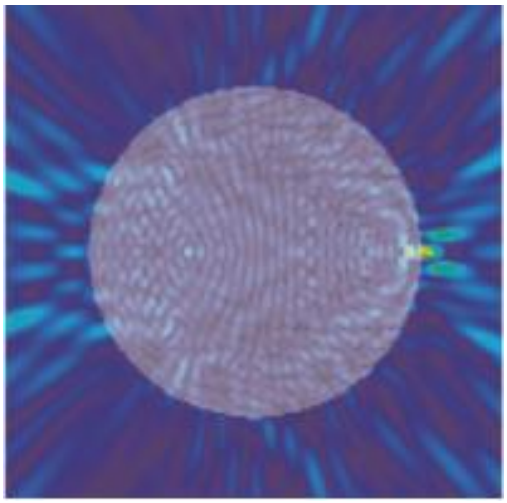

(b) Directional emission obtained using a point-scatterer [35]

Figure 4.2: Resonators altered to give directional emission. In (a), the red corresponds to larger electric field, the blue with smaller. By deforming, we have four branches of higher intensity (in green), where the circle would have none. A similar ray in seen in (b) the right side.

considered a finite-size circular scatterer in the center of the disk, as in Figure 3.1. We discuss the solving of such a system in the next subsection.

4.2 Solving the equations

We assume the system is flat, so that we only need to consider transverse modes. These consist of two types; the transverse magnetic modes (TM) for which $H_z = 0$ and the transverse electric modes (TE) for which $E_z = 0$. We will only consider TM modes here.

Also, we assume the dielectric to be nonmagnetic so that $\boldsymbol{B} = \boldsymbol{H}$. Using cylindrical coordinates, we get the following equation for E_z as in [35]:

$$\frac{\partial^2 E_z}{\partial r^2} + \frac{1}{r}\frac{\partial E_z}{\partial r} + \frac{1}{r^2}\frac{\partial^2 E_z}{\partial \phi^2} + k^2 n^2(r,\phi) E_z = 0 \tag{4.1}$$

where k is the wave-number and $n(r,\phi)$ the effective position dependent refractive index[13]. This is a wave-equation that can be solved given appropriate boundary conditions, which are very similar to the previous system in Section 3. One condition is that we want the value of E_z to be finite for $r = 0$ since it would make physically no sense if it isn't. Also outgoing boundary conditions are imposed, which is $E_z(r) \propto e^{ikr}/\sqrt{r}$ as $r \to \infty$. The last thing is that we impose continuity of $E_z(r)$ and its derivative at the boundary of the resonator at a radius R and R_1. We can separate the equation as we did before and similarly conclude that the solutions are Bessel functions with argument $n(r)kr$. We pick the refractive index $n > 1$ for the microdisk in a medium with index 1. The scatterer inside it has index n_s.

The solution is very much like the previous, but the outside part is replaced by a Hankel function for the outgoing wave condition (see also [37]):

$$E_z = \begin{cases} A_m J_m(n_s kr) e^{\pm im\phi} & \text{if } r < R_1 \\ [B_m J_m(nkr) + C_m Y_m(nkr)] e^{\pm im\phi} & \text{if } R_1 < r < R \\ D_m H_m(kr) e^{\pm im\phi} & \text{if } r > R \end{cases}$$

where J_m and Y_m are Bessel functions of the first and second kind respectively, and H_m is the Hankel function of the first kind. The coefficients A_m, B_m, C_m, D_m represent the amplitudes of the electric field.

As before, we require the field and its radial derivative to be continuous at the boundaries, so we get in total four equations. These equations can be summarized in a homogeneous matrix equation:

$$\begin{pmatrix} J_m(n_s kR_1) & -J_m(nkR_1) & -nY_m(nkR_1) & 0 \\ n_s J'_m(n_s kR_1) & -nJ'_m(nkR_1) & -nY'_m(nkR_1) & 0 \\ 0 & J_m(nkR) & Y_m(nkR) & -H_m(kR) \\ 0 & nJ'_m(nkR) & nY'_m(nkR) & -H'_m(kR) \end{pmatrix} \begin{pmatrix} A_m \\ B_m \\ C_m \\ D_m \end{pmatrix} = \begin{pmatrix} 0 \\ 0 \\ 0 \\ 0 \end{pmatrix}.$$

[13] The refractive index needs to be corrected for the thickness of the material, which determines which modes can occur, see [36]

A resonance requires the existence of a non-trivial solution of this system, and so we must set the determinant of the matrix equal to zero. Using the identity $J'_m(z) = J_{m-1}(z) - \frac{m}{z}J_m(z)$ [28] to remove the derivative (effectively by lowering the corresponding index by 1), the condition can be written as:

$$\begin{aligned}
&[n_s J_m(nkR_1)J_{m-1}(n_s kR_1) - nJ_m(n_s kR_1)J_{m-1}(nkR_1)] \\
&\quad [nH_m(kR)Y_{m-1}(nkR) - Y_m(nkR)H_{m-1}(kR)] \\
&- [n_s Y_m(nkR_1)J_{m-1}(n_s kR_1) - nJ_m(n_s kR_1)Y_{m-1}(nkR_1)] \\
&\quad [nH_m(kR)J_{m-1}(nkR) - J_m(nkR)H_{m-1}(kR)] \\
&= 0.
\end{aligned} \tag{4.2}$$

To solve the equation numerically, one can again use a Newton procedure. However, considering the classical analogue in the next subsection, we will see that the spectrum in general will not show monodromy.

4.3 Presence of monodromy

To obtain the classical analogue, one can rewrite Equation (4.1). As a light-wave is not just a particle, we must be careful. A safe procedure is to derive the potential and interpret it. Using the separation $E_z(r,\phi) = \psi(r)\Phi(\phi)$, we can do the following steps:

$$\begin{aligned}
\nabla^2 E_z + k^2 n^2(r) E_z &= 0 \\
\implies \left[\frac{d^2}{dr^2} + \frac{1}{r}\frac{d}{dr}\right] E_z + \frac{1}{r^2}\frac{d^2}{d\phi^2} E_z + k^2 n^2(r) E_z &= 0 \\
\implies \left[\frac{d^2}{dr^2} + \frac{1}{r}\frac{d}{dr}\right] \psi\Phi - \frac{m^2}{r^2}\psi\Phi + k^2 n^2(r)\psi\Phi &= 0 \\
\implies -\left[\frac{d^2}{dr^2} + \frac{1}{r}\frac{d}{dr}\right] \psi + V_{\text{eff}}\psi &= E\psi
\end{aligned}$$

We note that this equation is similar to the Schrödinger equation[14], where we defined

$$\begin{aligned}
V_{\text{eff}} &= k^2(1 - n^2(r)) + \frac{m^2}{r^2} \\
E &= k^2
\end{aligned}$$

under the condition that the wavenumber k and energy E are real since we are dealing with a scattering problem. Hence the classical analogue is given by an effective potential defined as:

$$V_{\text{eff}}(m, r, E) = E(1 - n^2(r)) + \frac{m^2}{r^2}.$$

[14] A more formal way is to derive from the optical system a quantum system, and from the quantum system a classical system (optical → quantum → classical). As we do not treat (or need) the quantum system for the resonator, we skip it (so just: optical → classical).

This potential allows us to draw phase portraits, for which we now discuss some realistic system parameters.
For the refractive index of the disk, we pick $n = 3$, which is a typical value for a semiconductor. The scatterer is made of metal, which we assume to have an imaginary refractive index. We will not yet specify the index of the scatterer n_s. Again, R is scaled away, so we set it 1. For the size of the scatterer, R_1, we pick 0.5 in units of R. Inserting the discussed parameters gives us the following effective potential:

$$V_{\text{eff}}(m, r, E) = \begin{cases} E(1 - n_s^2) + m^2/r^2 & \text{if } 0 \leq r < 0.5 \\ -8E + m^2/r^2 & \text{if } 0.5 < r < 1 \\ m^2/r^2 & \text{if } r > 1 \end{cases}$$

Hence we can obtain the phase portrait for the system by plotting

$$p(m, r, E) = \pm\sqrt{2(E - V_{\text{eff}}(m, r, E))}$$

versus r, as done in Figure 4.3. The most likely candidate for monodromy is an isolated singularity. This would occur at the axis $m = 0$ since there the bifurcation occurs, in the way that then phase portraits consists of piecewise constant functions, which does not happen for $m \neq 0$. The argumentation is similar to that of the previous system. However, in this case for zero momentum, the potential and energy are related by a *constant* factor $1 - n_s^2$, meaning that we are always above or always below the barrier. This means that we cannot cross it, and so the motion in all pictures are thus the same and so we cannot have a problem with the action-angle variables. Hence we will not see monodromy under the initial assumptions.

In fact, this does not depend on the configuration. The potential (for zero angular momentum) will have a maximum (or at least a supremum), and at this value of the potential $V = cE$ where c is a constant. In our case c was $1 - n_s^2$. Now if $c > 1$, energies will always hit a potential barrier, and when $c < 1$, the wave always passes over it. The case $c = 1$ reduces to $c > 1$. Hence, using these set-ups, you will never have monodromy in optical microresonators. The only way to have monodromy is by letting the refractive index also depend on wavelength (and so energy) in a special way.

Consider again the potential, at a certain radial distance r_0. The ratio $V/E = c$ must then pass 1 when varying k. This means that $n^2(k, r_0)$ must pass 0 for some k, so the index should be able to go from real to imaginary. We assumed earlier that an index was either real or imaginary, but that is often not true. However, including the fact that a general index is complex does not solve our problem. We need that with varying k, the ratio of real and imaginary part passes 1. That is

$$\frac{n_r}{n_i} < 1 \text{ for small } k$$
$$\frac{n_r}{n_i} > 1 \text{ for large } k$$

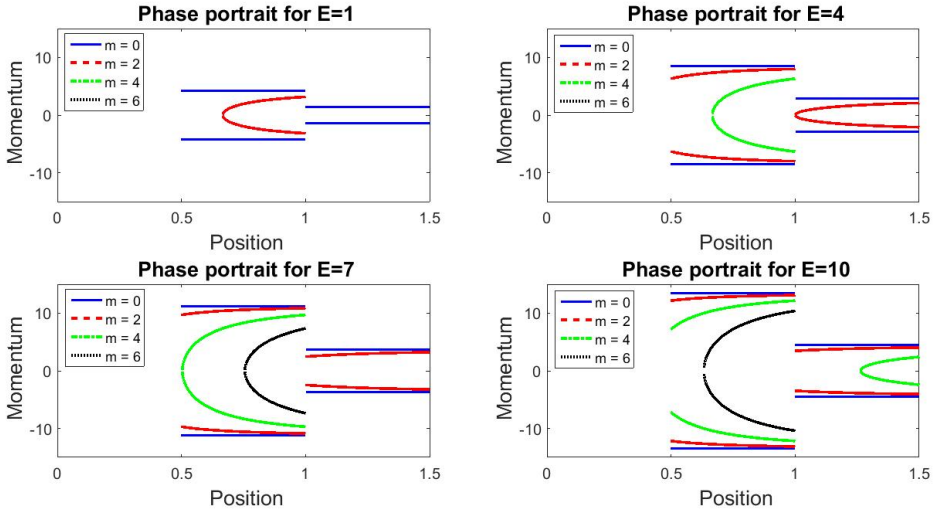

Figure 4.3: Curves for fixed energy E. The lines correspond to increasing values of m. The outer flat ones have $m = 0$, and in steps of 2 we move inwards. More values of m can be seen for larger E, but the qualitative pictures remain the same.

A search for typical materials has not brought forth a possible candidate [38]. We assume that we would need a custom material, and leave it as open question whether this is even possible.

5 Conclusion

We started this thesis with an introduction to monodromy. This included action-angle variables, classical and quantum interpretation of monodromy and the monodromy matrix. We proceeded by discussing examples of systems with monodromy and how to actually measure it in an experiment.

This introduction was used to treat a particular quantum system, namely the billiard. We found the spectra of the system, both using direct ways and WKB approximation. Monodromy was shown to be present, and we considered the classical analoque of the system to show it rigorously. We investigated the corresponding billiard map, phase portraits and action-angle variables. The latter was shown not to be able to be both globally smooth and single-valued, implying monodromy.

A similar quest was set out for the optical microresonator, but the particular dependence of the potential on the energy made it impossible to have monodromy using standard materials. We leave if as an open question whether or not a suitable material can be made.

6 References

[1] H. Waalkens, "Scattering monodromy in the two center problem." April 2014.

[2] V. I. Arnold, *Mathematical methods of classical mechanics*, vol. 60. Springer Science & Business Media, 1989.

[3] H. R. Dullin and H. Waalkens, "Nonuniqueness of the phase shift in central scattering due to monodromy," *Physical review letters*, vol. 101, no. 7, p. 070405, 2008.

[4] H. Waalkens and H. R. Dullin, "Quantum monodromy in prolate ellipsoidal billiards," *Annals of Physics*, vol. 295, no. 1, pp. 81–112, 2002.

[5] V. Guillemin and A. Uribe, "Monodromy in the quantum spherical pendulum," *Communications in mathematical physics*, vol. 122, no. 4, pp. 563–574, 1989.

[6] R. Cushman and J. Duistermaat, "The quantum mechanical spherical pendulum," *Bulletin of the American Mathematical Society*, vol. 19, no. 2, pp. 475–479, 1988.

[7] H. Waalkens, H. R. Dullin, and P. H. Richter, "The problem of two fixed centers: bifurcations, actions, monodromy," *Physica D: Nonlinear Phenomena*, vol. 196, no. 3, pp. 265–310, 2004.

[8] B. Zhilinskii, "Hamiltonian monodromy, its manifestations and generalizations," *Research Institute for Mathematical Sciences, Kyoto University*, vol. 1692, pp. 57–77, 2010.

[9] J. J. Duistermaat, "On global action-angle coordinates," *Communications on pure and applied mathematics*, vol. 33, no. 6, pp. 687–706, 1980.

[10] N. Sansonetto and M. Spera, "Hamiltonian monodromy via geometric quantization and theta functions," *Journal of Geometry and Physics*, vol. 60, no. 3, pp. 501–512, 2010.

[11] B. Zhilinskii, "Hamiltonian monodromy as lattice defect," in *Topology in Condensed matter*, pp. 165–186, Springer, 2006.

[12] N. F. Zobov *et al.*, "Monodromy in the water molecule," *Chemical physics letters*, vol. 414, no. 1, pp. 193–197, 2005.

[13] M. Child, "Quantum monodromy and molecular spectroscopy," *Contemporary Physics*, vol. 55, no. 3, pp. 212–221, 2014.

[14] J. B. Delos, G. Dhont, D. A. Sadovskii, and B. I. Zhilinskii, "Dynamical manifestation of Hamiltonian monodromy," *EPL (Europhysics Letters)*, vol. 83, no. 2, p. 24003, 2008.

[15] S. Vũ Ngoc, "Quantum monodromy in integrable systems," *Communications in mathematical physics*, vol. 203, pp. 465–479, 1999.

[16] M. Child, T. Weston, and J. Tennyson, "Quantum monodromy in the spectrum of H2O and other systems: new insight into the level structure of quasi-linear molecules," *Molecular Physics*, vol. 96, no. 3, pp. 371–379, 1999.

[17] M. Joyeux, D. Sadovskıı, and J. Tennyson, "Monodromy of the LiNC/NCLi molecule," *Chemical physics letters*, vol. 382, no. 3, pp. 439–442, 2003.

[18] R. H. Cushman and L. M. Bates, *Global aspects of classical integrable systems*. Birkhäuser, 2012.

[19] R. Cushman and D. Sadovskıı, "Monodromy in the hydrogen atom in crossed fields," *Physica D: Nonlinear Phenomena*, vol. 142, no. 1, pp. 166–196, 2000.

[20] M. Sanrey, M. Joyeux, and D. A. Sadovskii, "Classical and quantum-mechanical plane switching in CO2," *The Journal of chemical physics*, vol. 124, no. 7, p. 074318, 2006.

[21] A. J. Nozik *et al.*, "Semiconductor quantum dots and quantum dot arrays and applications of multiple exciton generation to third-generation photovoltaic solar

cells," *Chemical reviews*, vol. 110, no. 11, pp. 6873–6890, 2010.

[22] M. I. Katsnelson, K. S. Novoselov, and A. K. Geim, "Chiral tunnelling and the Klein paradox in graphene," *Nature physics*, vol. 2, no. 9, pp. 620–625, 2006.

[23] S. Pathak *et al.*, "Quantum dot applications to neuroscience: new tools for probing neurons and glia," *The Journal of neuroscience*, vol. 26, no. 7, pp. 1893–1895, 2006.

[24] A. Samia, S. Dayal, and C. Burda, "Quantum dot-based energy transfer: Perspectives and potential for applications in photodynamic therapy," *Photochemistry and photobiology*, vol. 82, no. 3, pp. 617–625, 2006.

[25] A. Kiraz, M. Atatüre, and A. Imamoğlu, "Quantum-dot single-photon sources: Prospects for applications in linear optics quantum-information processing," *Physical Review A*, vol. 69, no. 3, p. 032305, 2004.

[26] M. A. Nielsen and I. L. Chuang, *Quantum computation and quantum information*. Cambridge university press, 2010.

[27] M. Hentschel and K. Richter, "Quantum chaos in optical systems: the annular billiard," *Physical Review E*, vol. 66, no. 5, p. 056207, 2002.

[28] M. Abramowitz and I. A. Stegun, *Handbook of mathematical functions: with formulas, graphs, and mathematical tables*. No. 55, Courier Corporation, 1964.

[29] D. J. Griffiths, *Introduction to Quantum Mechanics*. Pearson, July 2013.

[30] K. J. Vahala, "Optical microcavities," *Nature*, vol. 424, no. 6950, pp. 839–846, 2003.

[31] D. Kleppner, "Inhibited spontaneous emission," *Physical Review Letters*, vol. 47, no. 4, p. 233, 1981.

[32] S. B. Alexander *et al.*, "A precompetitive consortium on wide-band all-optical networks," *Journal of Lightwave Technology*, vol. 11, no. 5, pp. 714–735, 1993.

[33] J. U. Nöckel and A. D. Stone, "Ray and wave chaos in asymmetric resonant optical cavities," *arXiv preprint chao-dyn/9806017*, 1998.

[34] J. Heebner, R. Grover, T. Ibrahim, and T. A. Ibrahim, *Optical microresonators: theory, fabrication, and applications*. Springer Science & Business Media, 2007.

[35] C. P. Dettmann, G. Morozov, M. Sieber, and H. Waalkens, "Unidirectional emission from circular dielectric microresonators with a point scatterer," *Physical Review A*, vol. 80, no. 6, p. 063813, 2009.

[36] M. Lebental *et al.*, "Inferring periodic orbits from spectra of simply shaped microlasers," *Physical Review A*, vol. 76, no. 2, p. 023830, 2007.

[37] J. Sun, M. Huang, J.-J. Yang, T.-H. Li, and Y.-Z. Lan, "A microring resonator based negative permeability metamaterial sensor," *Sensors*, vol. 11, no. 8, pp. 8060–8071, 2011.

[38] M. Polyanskiy, "Refractiveindex.info." `http://refractiveindex,info`, 2015. Accessed Spring/Summer 2015.

A Derivation of the billiard map

Let's start by considering free motion in a disk or radius R (so without potential barrier). We naturally parametrize the boundary circle by its arclength s (and take it modulo $2\pi R$), and we choose $\phi \in [0, \pi]$ to be the angle between the forward trajectory of the particle and the (counterclockwise) tangent to the circle, see Figure A.1.

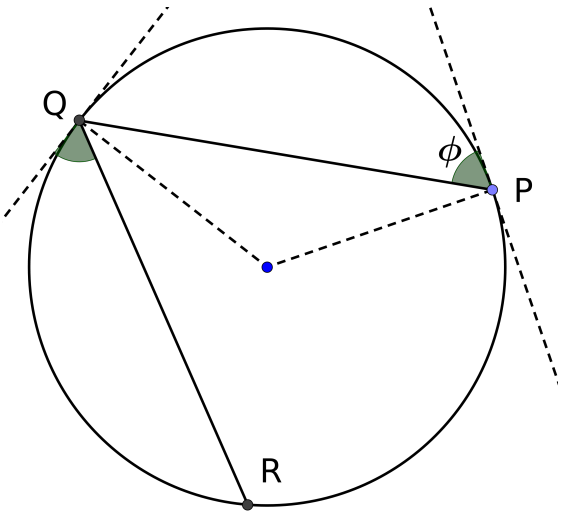

Figure A.1: A particle starting in P is reflected in Q and moves on to R. The definition of ϕ is as indicated, and this angle is conserved.

We note that this angle is directly related to the angular momentum; since $l = r \times p$, we have $l = Rmv \sin(\pi/2 + \phi) = Rmv \cos(\phi)$. For a given energy E, we know that

$$E = \frac{1}{2m}\left(p_r^2 + \frac{l^2}{r^2}\right) + V.$$

We get maximal angular momentum if the radial momentum, p_r, is zero and we have a maximal radial distance, which is R. Since the potential is zero in this region, we can find that

$$l_{\max} = R\sqrt{2mE} = Rmv.$$

So if we measure momentum relative to this maximum, the result is simply $l = \cos(\phi)$. Indeed, when the particle moves directly towards the center, we have $\phi = \pi/2$ and $l = 0$, while a particle 'moving along' the boundary in positive direction has $\phi = 0$ and $l = 1$. When moving along the boundary in opposite direction, we have $\phi = \pi$ and hence $l = -1$.

The angle ϕ is conserved by the billiard map; this can be seen using the symmetry of the system or appealing to conservation of $l = \cos(\phi)$. The angle between the points of reflection can be found to be 2ϕ, and so the increase of s equals $2\phi R$. The billiard

map has as inputs the arc-length s and the momentum $l = \cos(\phi)$, so for the circle, the billiard map is

$$(s, \cos(\phi)) \mapsto (s + 2\phi R \mod 2\pi R, \cos(\phi)) \tag{A.1}$$

where the domain is $[0, 2\pi R) \times [-1, 1]$. This is of course also the range, and it is topologically a cylinder ($\mathbb{S}^1 \times I$ where I is an interval).

Now it might be impossible for the particle to reach a center disk because it has too little energy. So, the particle can move only in a annulus (flat torus) and the billiard map corresponding to it is the annular billiard. This map will consist of two cases; hitting the center disk or not. If we do not hit it, we have the circular billiard in Equation (A.1). If the inner disk has radius R_1, the critical angle is defined by $\sin(\pi/2 - \phi_c) = R_1/R$ and so equals

$$\phi_c = \cos^{-1}(R_1/R).$$

Hence we can resort to Equation (A.1) if $\phi \notin [\phi_c, \pi - \phi_c]$. To derive the other part of the map, we can use the conservation of angular momentum. Let θ be the angle under which the particle hits (and leaves) the inner disk with respect to the tangent of the inner disk, see Figure A.2.

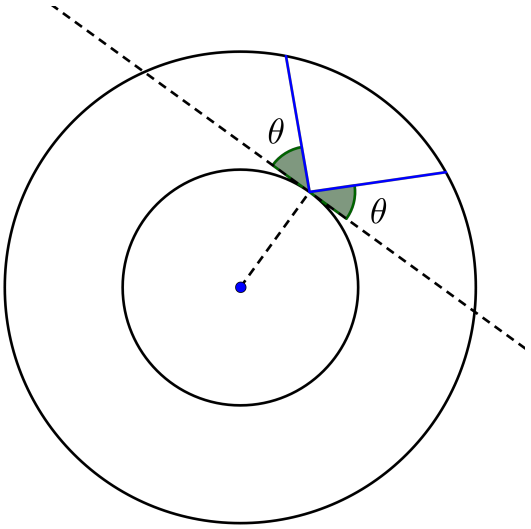

Figure A.2: A particle is deflected when reaching the inner disk, coming in (and leaving) under an angle θ.

When the particle hits the disk, it momentum equals $l' = R_1 mv \cos(\theta)$. Since $l = Rmv \cos(\phi)$ and $l = l'$, we see that $R\cos(\phi) = R_1 \cos(\theta)$ and so

$$\theta = \cos^{-1}\left(\frac{R}{R_1}\cos(\phi)\right).$$

Consider the triangle formed by the center, the point of first reflection (at $r = R$)

and the point where the particle hits the inner disk (at $r = R_1$). One of the angles in this triangle is the increase in polar angle of the particle, which we call Δs, as in Figure A.3.

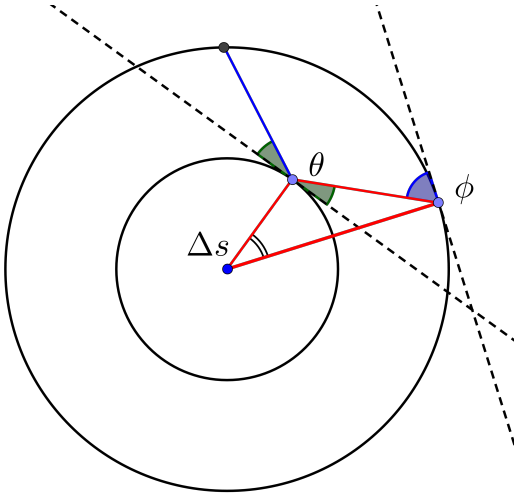

Figure A.3: Calculating the change in polar angle (Δs) due to deflection by the inner disk.

The Triangle Sum Theorem states then

$$\Delta s + \frac{\pi}{2} + \theta + \frac{\pi}{2} - \phi = \pi$$

which is easily solved for Δs, and equals $\Delta s = \phi - \theta$. During the time it takes for the particle to reach the outer boundary again, the polar angle will again increase by Δs, and so map for hitting the inner disk is given by

$$(s, \cos(\phi)) \mapsto \left(s + 2\phi R - 2R\cos^{-1}\left(\frac{R}{R_1}\cos(\phi)\right), \cos(\phi)\right) \tag{A.2}$$

and hence the full annular billiard map is found by combining Equations (A.1) and (A.2) to give:

$$(s, \cos(\phi)) \mapsto \begin{cases} (s + 2\phi R, \cos(\phi)) & \text{if } \phi \notin [\phi_c, \pi - \phi_c] \\ \left(s + 2\phi R - 2R\cos^{-1}\left(\frac{R}{R_1}\cos(\phi)\right), \cos(\phi)\right) & \text{if } \phi \in [\phi_c, \pi - \phi_c] \end{cases} \tag{A.3}$$

The annular billiard can be extended further by implementing a finite potential barrier in the inner disk, instead of an infinite barrier. Particles with sufficiently high energies may then penetrate the inner disk, while experiencing refraction. In order to get the new billiard map (which does now also depend on energy), we need to qualify the refraction relation. Let the potential barrier have a height of V_0. The angular momentum

outside the disk we already know how to calculate (as we did for the outer disk), and equals

$$l_{\text{out}} = R_1\sqrt{2mE}\cos(\theta)$$

using $E = p^2/2m + V$. If the particle enters the inner disk with an angle α relative to the tangent, its angular momentum now equals

$$l_{\text{in}} = R_1\sqrt{2m(E - V_0)}\cos(\alpha).$$

Using conservation of angular momentum, we may write

$$\frac{\cos(\alpha)}{\cos(\theta)} = \sqrt{\frac{E}{E - V_0}}$$

or

$$\alpha = \cos^{-1}\left(\cos(\theta)\sqrt{\frac{E}{E - V_0}}\right). \tag{A.4}$$

We see that $E > V_0$ does not guarantee that the particle will enter the inner disk. To this end, the argument of the $\cos^{-1}$ has to be smaller than 1 in absolute value. Otherwise, the particle will undergo total internal reflection.

Having deduced all the relevant refraction angles, we can calculate the increase in s for the case that we have refraction in the inner disk.

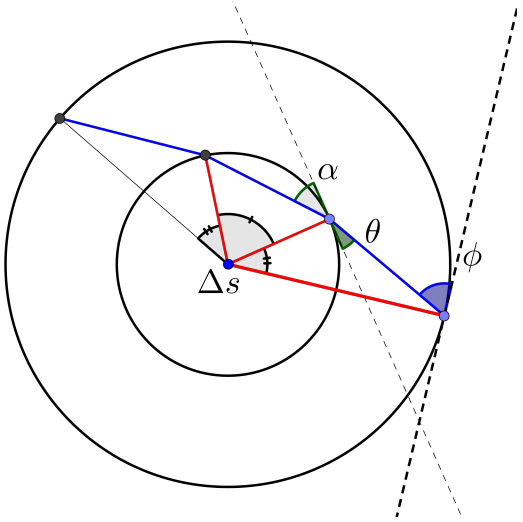

Figure A.4: A particle is refracted by the inner disk. We see $\Delta s = s_1 + 2s_2$ where s_1 is the change in angle while traveling through the inner disk (marked by one stripe) and s_2 (marked by two stripes) the previous Δs.

Looking at Figure A.4, consider the triangle formed by the center and the points

where the particle crosses the inner boundary[15]. The Triangle Sum Theorem then states

$$s_1 + 2\left(\frac{\pi}{2} - \alpha\right) = \pi.$$

and hence $s_1 = 2\alpha$. The total increase equals $\Delta s = s_1 + 2s_2 = 2\alpha + 2(\phi - \theta)$, giving us the last result we need. Hence the complete billiard map is (only considering the arc-length since both angular momentum and energy are conserved):

$$s \mapsto \begin{cases} s + 2\phi R & \text{if } \phi \notin [\phi_c, \pi - \phi_c] \\ s + 2(\phi - \theta + \alpha)R & \text{if } \phi \in [\phi_c, \pi - \phi_c] \text{ and } E > V_0 \wedge |\cos(\theta)| \leq \sqrt{1 - \frac{V_0}{E}} \\ s + 2(\phi - \theta)R & \text{otherwise} \end{cases} \tag{A.5}$$

where the additional angles are defined as

$$\begin{aligned} \phi_c &= \cos^{-1}\left(\frac{R_1}{R}\right) \\ \theta &= \cos^{-1}\left(\frac{R}{R_1}\cos(\phi)\right) \\ \alpha &= \cos^{-1}\left(\cos(\theta)\sqrt{\frac{E}{E - V_0}}\right). \end{aligned} \tag{A.6}$$

In the last case, the points where the particle crosses the boundary are given by polar angles $s/R + \phi - \theta$ and $s/R + \phi - \theta + 2\alpha$. The case $E = V_0$ is special; there is normal movement if the inner disk is not hit, but a particle hitting it would come to a sudden stand-still at $r = R_1$ (or it occupies some location inside the inner disk with zero velocity).

[15] It depends on the sign of V_0 whether the particle is bend towards the normal or not. In this case, the potential is negative resulting in a wide picture enabling a clear view on the situation.